AD-A118 946 SYSTEMS RESEARCH LABS INC DAYTON OH F/G 11/2
MECHANISMS OF DUCTILITY AND FRACTURE IN HIGH-TEMPERATURE MATERI--ETC(U)
JUN 82 M G MENDIRATTA, T MAH, D K CHATTERGEE F33615-78-C-5037
UNCLASSIFIED SRL-6985 AFWAL-TR-82-4061 NL

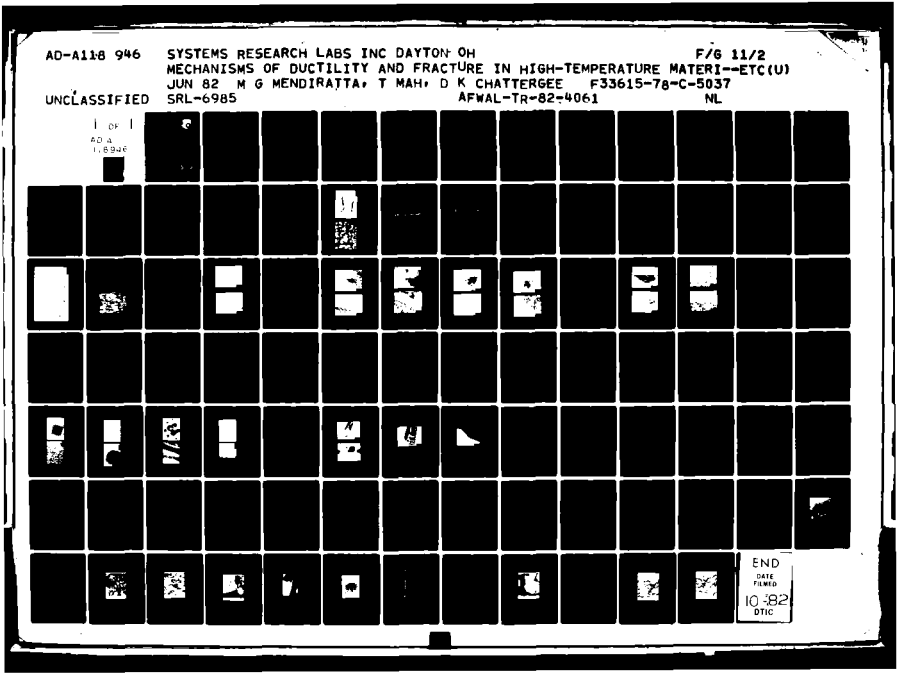

AFWAL-TR-82-4061

MECHANISMS OF DUCTILITY AND FRACTURE IN HIGH-TEMPERATURE MATERIALS

M. G. Mendiratta, Ph.D.
Tai-Il Mah, Ph.D.
D. K. Chatterjee, Ph.D.

Research Applications Division
Systems Research Laboratories, Inc.
2800 Indian Ripple Road
Dayton, OH 45440

June 1982

Final Technical Report for Period 3 April 1978 - 1 August 1981

MATERIALS LABORATORY
AIR FORCE WRIGHT AERONAUTICAL LABORATORIES
AIR FORCE SYSTEMS COMMAND
WRIGHT-PATTERSON AIR FORCE BASE, OHIO 45433

NOTICE

When Government drawings, specifications, or other data are used for any purpose other than in connection with a definitely related Government procurement operation, the United States Government thereby incurs no responsibility nor any obligation whatsoever; and the fact that the government may have formulated, furnished, or in any way supplied the said drawings, specifications, or other data, is not to be regarded by implication or otherwise as in any manner licensing the holder or any other person or corporation, or conveying any rights or permission to manufacture, use, or sell any patented invention that may in any way be related thereto.

This report has been reviewed by the Office of Public Affairs (ASD/PA) and is releasable to the National Technical Information Service (NTIS). At NTIS, it will be available to the general public, including foreign nations.

This technical report has been reviewed and is approved for publication.

HARRY A. LIEBITT
Project Engineer

NORMAN M. GEYER
Technical Area Manager
Processing & High Temperature
Materials Branch
Metals & Ceramics Division

FOR THE COMMANDER

HENRY C. GRAHAM, Chief
Processing & High Temperature
Materials Branch
Metals & Ceramics Division

"If your address has changed, if you wish to be removed from our mailing list, or if the addressee is no longer employed by your organization please notify AFWAL/MLLM *, W-PAFB, OH 45433 to help us maintain a current mailing list".*

Copies of this report should not be returned unless return is required by security considerations, contractual obligations, or notice on a specific document.

Unclassified

SECURITY CLASSIFICATION OF THIS PAGE *(When Data Entered)*

REPORT DOCUMENTATION PAGE		READ INSTRUCTIONS BEFORE COMPLETING FORM
1. REPORT NUMBER AFWAL-TR-82-4061	2. GOVT ACCESSION NO. AD-A118 946	3. RECIPIENT'S CATALOG NUMBER
4. TITLE *(and Subtitle)* Mechanisms of Ductility and Fracture in High-Temperature Materials		5. TYPE OF REPORT & PERIOD COVERED Final Technical Report 3 April 1978 - 1 August 1981
		6. PERFORMING ORG. REPORT NUMBER SRL - 6985 Final
7. AUTHOR(s) M. G. Mendiratta, Ph.D. Tai-Il Mah, Ph.D. D. K. Chatterjee, Ph.D.		8. CONTRACT OR GRANT NUMBER(s) F33615-78-C-5037
9. PERFORMING ORGANIZATION NAME AND ADDRESS Systems Research Laboratories, Inc. 2800 Indian Ripple Rd. Dayton, OH 45440		10. PROGRAM ELEMENT, PROJECT, TASK AREA & WORK UNIT NUMBERS 6.1102, 2306, 2306P1, 2306P105
11. CONTROLLING OFFICE NAME AND ADDRESS Air Force Wright Aeronautical Laboratories Materials Laboratory (AFWAL/MLLM) Wright-Patterson Air Force Base, OH 45433		12. REPORT DATE June 1982 13. NUMBER OF PAGES 94
14. MONITORING AGENCY NAME & ADDRESS *(if different from Controlling Office)*		15. SECURITY CLASS. *(of this report)* Unclassified 15a. DECLASSIFICATION/DOWNGRADING SCHEDULE

16. DISTRIBUTION STATEMENT *(of this Report)*

Approved for public release; distribution unlimited.

17. DISTRIBUTION STATEMENT *(of the abstract entered in Block 20, if different from Report)*

18. SUPPLEMENTARY NOTES

19. KEY WORDS *(Continue on reverse side if necessary and identify by block number)*

four-point-bend strength
fractography
slip systems
brittle/ductile transition
titanium carbide
brittle ceramic composite
iron-aluminide
alkoxy-derived mullite

20. ABSTRACT *(Continue on reverse side if necessary and identify by block number)*

Investigations have been carried out on the fabrication, microstructural characterization, and mechanical-property determination of TiC, brittle ceramic composites, iron aluminides, titanium aluminides, and mullite. The slip systems in TiC as a function of temperature were established by deforming single crystals; below 600°C, the slip system was $\{110\}\langle 1\bar{1}0\rangle$, above 800°C, it was $\{111\}\langle 1\bar{1}0\rangle$. At temperatures of 600 - 800°C, both slip systems were operative. Polycrystalline TiC was fabricated by hot-pressing commercially available

DD FORM 1 JAN 73 1473 EDITION OF 1 NOV 65 IS OBSOLETE

Unclassified

SECURITY CLASSIFICATION OF THIS PAGE *(When Data Entered)*

Abstract continued

TiC powders. The strength of the hot-pressed TiC dropped drastically above 1000°C. Fractography and bulk chemical analysis revealed the presence of low-melting metallic impurities--principally Fe and Co which segregated to the grain boundaries producing premature intergranular fracture at high temperatures. No ductility at any temperature was observed in the hot-pressed TiC. Heat treatments at temperatures greater than 2000°C decreased the metallic impurities significantly and provided some ductility at high temperatures. The B/D transition temperature was brought down to 800°C by 2300°C/4 hr heat treatment. A Si_3N_4-20 vol% TiC composite exhibited a 50% increase in fracture toughness over that of the Si_3N_4 matrix. Strength and toughness properties of glass + SiC (particulate) composites were measured, and the overall behavior was found to be similar to that of other similar systems--glass + Al_2O_3 particles. In iron aluminides, two alloys have been investigated--Fe-25 at% Al produced by utilizing RSR powders and Fe-31 at.% Al produced by vacuum arc melting. Both alloys were hot-extruded and heat-treated to produce equi-axed grain structure, and both exhibited reasonable levels of strength and ductility at room temperature. The deformation and fracture behavior of these alloys has been investigated. In titanium aluminides, the stress and temperature dependences of steady-state-creep rates of Ti_3Al- and TiAl-based alloys have been established. The strength and fracture behavior of alkoxy-derived mullite was investigated.

FOREWORD

This report was prepared by the Research Applications Division of Systems Research Laboratories, Inc., Dayton, Ohio, under Air Force Contract F33615-78-C-5037, Project 2306, Task P1, Work unit 05. Dr. H. A. Lipsitt of the Processing and High Temperature Materials Branch, Materials Laboratory (AFWAL/MLLM), Air Force Wright Aeronautical Laboratories, Wright-Patterson Air Force Base, Ohio, was the Government Project Monitor. The research reported herein covered the period 3 April 1978 through 1 August 1981.

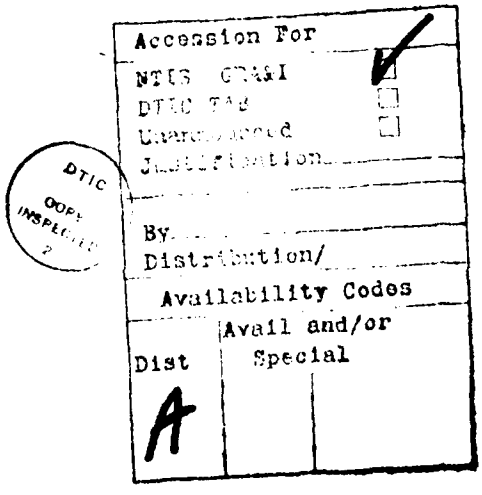

TABLE OF CONTENTS

LIST OF ILLUSTRATIONS

Section I

INTRODUCTION

Significant improvements in the performance of current gas-turbine engines are possible through the use of higher operating temperatures and lower-density structural materials. Currently used alloys based upon titanium, iron, nickel,and cobalt are rapidly approaching their developmental limit in terms of achieving increased temperature capabilities; therefore, efforts have been made to develop new classes of materials. The dual objective of higher operating temperatures and lower-density materials has prompted research efforts toward the development of ceramics and intermetallics, many of which exhibit low density, high strength, and inertness up to high temperatures.

At the Materials Laboratory, AF Wright Aeronautical Laboratories at Wright-Patterson Air Force Base, considerable research efforts are being directed toward development of various ceramic systems and iron and titanium aluminides for high-temperature applications. Systems Research Laboratories, Inc. (SRL), has participated in these programs and this report includes the results of investigations on the following five classes of materials:

1. Polycrystalline TiC
2. Brittle ceramic composites: Si_3N_4 + TiC particles and glass + SiC particles
3. Iron-aluminides
4. Titanium-aluminides
5. Mullite

One of the major problems with these materials is the lack of adequate room-temperature ductility and fracture toughness. The overall approach to these investigations was to gain an understanding of the mechanisms of the brittle/ductile (B/D) transition and toughening and to explore the possibility that by process control and/or alloying,either the B/D transition temperature could be lowered or the toughness increased. In addition

to the focus upon the problem of ductility and toughness, other important properties such as strength, creep, and oxidation resistance were also investigated over a wide range of temperatures.

A number of papers have resulted from these investigations. Those already published are listed herein, and two which have been submitted for publication appear in the Appendix. In addition to these papers, which essentially encompass the important aspects of the investigations, relevant additional data are also included in this report. Finally, summaries of major findings on each material system are given.

SECTION II

SUMMARY OF MAJOR FINDINGS

1. TITANIUM CARBIDE

Investigation of the plastic deformation of single-crystal TiC revealed that from room temperature to 600°C, the operative slip system is {110} <110>; above 800°C, it is {111} <110>. At temperatures between 600 and 800°C, both slip systems are operative. At temperatures higher than 800°C, extensive cross-slip occurs. It is suggested that this change of slip system and propensity for cross-slip are responsible for the B/D transition in polycrystalline TiC.

Near-theoretical-density polycrystalline TiC can be fabricated by hot-pressing commercially available TiC powders. However, the four-point-bend tensile strength of such materials was found to drop significantly above 1000°C. It was found that at testing temperatures higher than $1000^{\circ}C$, the metallic impurities--principally Co and Fe--form low-melting eutectics at the grain boundaries which are responsible for intergranular fracture at low stresses. Clear indication of the presence of the molten material was revealed by SEM fractography. In the as-hot-pressed material, ductility was not observed at any temperature.

Vacuum heat treatments of as-hot-pressed TiC at temperatures greater than $2000^{\circ}C$ improved the high-temperature strength and provided some degree of ductility. The B/D transition temperature was reduced to ~ $800^{\circ}C$ by vacuum annealing the as-hot-pressed TiC at $2300^{\circ}C$ for 4 hr. The transition temperature was found to be dependent upon grain size--the larger the grain size, the lower the B/D temperature. Bulk chemical analysis of the vacuum annealed specimens revealed that the metallic impurities Co and Fe were reduced significantly as compared to those in as-hot-pressed TiC. SEM fractography revealed the absence of molten material at the grain boundaries in the vacuum annealed specimens.

An investigation was carried out on irradiation damage caused in thin foils of TiC by low-energy electrons in the TEM. Instantaneous void formation in TiC was observed in localized areas of the thin foils of single crystals of $TiC_{0.93}$ irradiated by a 100-kV electron beam at temperatures of 800°C and above. This void formation was interpreted as being due to selective displacement of lighter carbon atoms by electron irradiation and is facilitated by substoichiometry and also by the prior microstructure of the TiC.

At the initial stage of electron irradiation, carbon atoms are displaced from the TiC lattice and deposited on the foil surface as graphite. As the irradiation continues, carbon vacancies, created during irradiation, order due to irradiation-induced diffusion, and a cubic superstructure having a lattice parameter of 9.2 Å forms in the TiC. However, with continued irradiation, the carbon atoms in this ordered superstructure are displaced by the impinging electrons, and a disordering of the superstructure results.

An investigation was carried out to study the early stages of oxidation of TiC. A single crystal of TiC having an (001) orientation was oxidized at 900°C in four different partial pressures of oxygen and examined by TEM. At higher partial pressures of oxygen, complete oxidation of TiC resulting in TiO_2 was observed; whereas, at lower partial pressures, only epitaxial oxides were formed. These expitaxial oxides consisted of both TiO and TiO_2 and their growth orientation relationship with TiC was established to be: $(002)_{TiC}||(002)_{TiO}$; $[002]_{TiC}||[002]_{TiO}$ and $(200)_{TiC}||(002)_{TiO_2}$; $[002]_{TiC}||[200]_{TiO_2}$. Bulk oxidation or grain-boundary oxidation of TiC was not evident at low partial pressures of oxygen.

2. BRITTLE CERAMIC COMPOSITES

Composites consisting of a Si_3N_4 matrix and different volume fractions of TiC particles (average size ~ 10 μm) were fabricated by hot pressing powder blends and employing 6 wt % CeO_2 as a hot-pressing aid. A maximum increase of 50% in fracture toughness over that in Si_3N_4 was exhibted by the

20 vol% TiC composite. Toughening was thought to be due to microcracking in the vicinity of the particles and crack bowing between the particles.

Investigations were carried out on glass + SiC particle composites, principally to become acquainted with fabrication techniques. The results were similar to those found for other similar systems (glass-Al_2O_3 particle) investigated previously. Detailed results are given in Section III.

3. IRON-ALUMINIDES

Research efforts on iron-aluminides consisted of processing and fabrication of alloy billets having the composition Fe-25 at% and higher Al content by conventional ingot-metallurgy and powder-metallurgy techniques and characterizing these billets for microstructures and mechanical properties. Extreme difficulties were encountered in producing sound, pore-free castings. Also, various combinations of conventional forging and heat treating did not provide desirable microstructures in the castings. The grain size of these alloys was quite large and nonuniform (size range 600-800 μm). Hot extrusion was successfully used to produce equi-axed grains (size ~ 150 μm) in the cast Fe-31 at% Al alloy. However, hot extrusion of RSR powders of various binary iron-aluminide compositions produced an extremely uniform microstructure consisting of equi-axed grains having an average size in the range ~ 40-50 μm.

The hot-extruded RSR Fe-25 at% Al alloy exhibited a good combination of room-temperature tensile properties. The cast and hot-extruded Fe-31 at% Al alloy also exhibited a reasonable combination of room-temperature tensile properties. The plastic deformation was provided predominantly by the motion and cross-slip of ordinary dislocations (and not superlattice dislocations) which created anti-phase boundary ribbons. Fracture occurred by transgranular cleavage.

4. TITANIUM-ALUMINIDES

The stress and temperature dependences of the steady-state creep rates of Ti_3Al- and TiAl-based alloys were established; from these, the activation energies and stress exponents were calculated.

Section III

ADDITIONAL INVESTIGATIONS

1. POLYCRYSTALLINE TITANIUM CARBIDES

For the past three years, SRL has been investigating deformation and fracture behavior of polycrystalline titanium carbides made from powders purchased from various sources. Commercial titanium-carbide powders were purchased from Refractory Metals, Inc., Ventron Corp., and H. C. Starck Co. Powders were consolidated through conventional hot-pressing techniques and near-theoretical densities were achieved without difficulty. Table I shows the impurity content of three starting powders and their average particle size.

The hot-pressed samples were subjected to four-point-bend tests both at room temperature and at elevated temperatures. The room-temperature fracture strength was retained up to ~ 600°C for TiC made from RMI powders which were sieved through Cu screens. Without sieving through Cu screens, the strength was retained up to 1000°C. Above these temperatures the fracture strength dropped drastically with increasing temperature. The mode of fracture was predominantly transgranular cleavage at room temperature with a transition in the mode to intergranular fracture at temperatures where strength begins to decrease. The fracture mode was completely intergranular at high temperatures. This behavior can be rationalized by means of Fig. 1 which shows schematically the dependence of T_{BD} upon the competition between yield and fracture strength. The figure also includes another curve which schematically shows the variation of the grain-boundary strength. All of the polycrystalline titanium carbides tested in the as-hot-pressed condition thus failed prematurely at high temperatures before exhibiting plastic yielding. The temperature dependence of the grain-boundary strength is mainly governed by the segregation of specific impurities, the most detrimental elements being Cu, Fe, Co, and Cr. The fracture surfaces were examined by scanning Auger microscopy,* and the typical microscopic

*Super-SAM Model 590.

TABLE I

IMPURITY CONTENT AND AVERAGE PARTICLE SIZE
OF STARTING POWDERS FROM THREE SOURCES

	RMI	Ventron	Starck
Si	200	100	20
Mg	10	2	5
Mn	20	2	7
Al	20	<20	20
Fe	2000	500	300
Ni	10	20	50
Cr	500	500	500
Co	20	2000	500
W	2000	5000	3000
Ca	20	20	30
Mo	20	20	100
Zr	20	20	10
Carbon	19.1,19.0	19.1619.3,19.4	19.44
oxygen	0.242,0.165	0.283,0.141,0,159	0.159
	200 u to 2 µ	-325 mesh	- 325 mesh

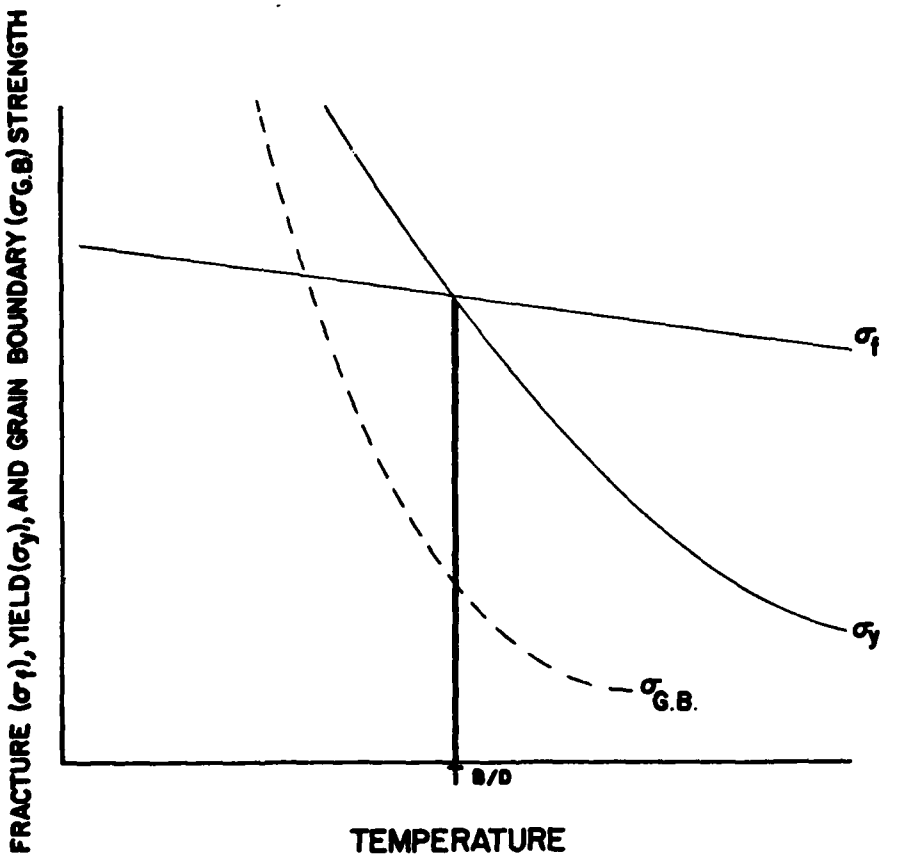

Figure 1. Schematic Representation of the Competition between Cleavage and Grain-Boundary-Fracture Strengths and Yield Strength as a Function of Temperature.

features are shown in Fig. 2 (a-b) along with the energy-dispersive spectra* [Fig. 2(c)]. The high-temperature intergranularly fractured RMI specimen exhibits a very high concentration of copper and iron. The copper contamination occurred as a result of the sieving process, and other impurities were present in the powder. Direct comparison between the chemistry of the grain boundaries and the cleavage planes can be made by a comparison of Figs. 2 and 3; the latter is taken from a cleavage facet and the cleavage planes. Ventron and Starck materials behave similarly in terms of mechanical properties and impurity effects. Starck materials are discussed in further detail in the Appendix. Through the proper choice of heat treatment, the impurity levels were decreased considerably, and the grain boundaries were strengthened. After heat treatment the hypothetical $\sigma_{G.B.}$ curve can be considered to shift toward higher temperature, past the σ_y curve in the figure, suggesting the possibility of plastic deformation in polycrystalline TiC. The effects of heat treatment upon the mechanical and microstructural behavior of TiC are described in the SRL Interim Quarterly Reports under this contract as well as in the publications appearing in the Appendix.

2. BOROSILICATE GLASS - SiC PARTICLE COMPOSITES

Because of the extreme brittleness of ceramics, crack propagation in these materials requires a very low expenditure of energy, i.e., these materials possess low fracture toughness. It is of considerable basic, as well as practical, importance to understand the toughening mechanisms--especially the role of microstructural parameters in influencing fracture toughness. In an attempt to gain an understanding of toughening, preliminary studies were carried out on glass - SiC particle composites--considered to be a model system for hard-particle-dispersion toughening.

---

*Furnished by Dr. A. Katz of AFWAL/MLLM.

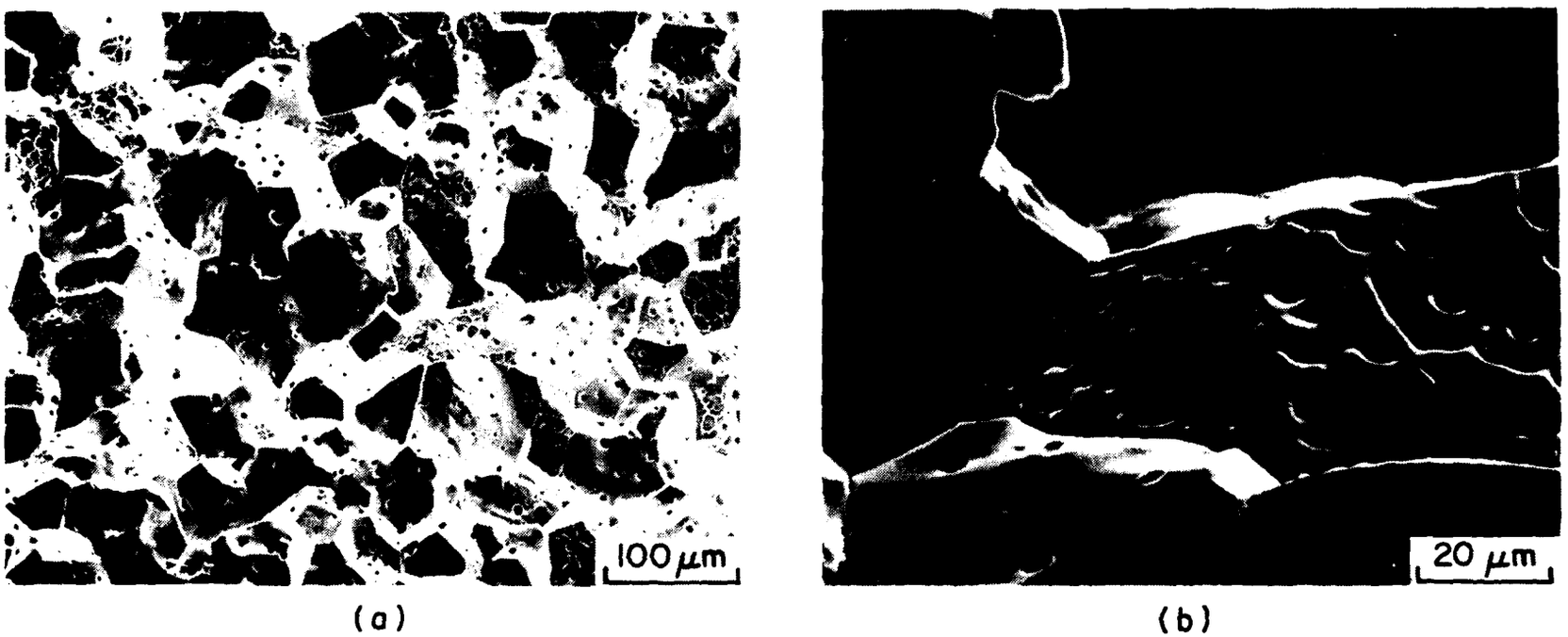

Figure 2. (a,b) SEM Fratographs and (c) Auger Chemical Analysis of Intergranular Fracture.

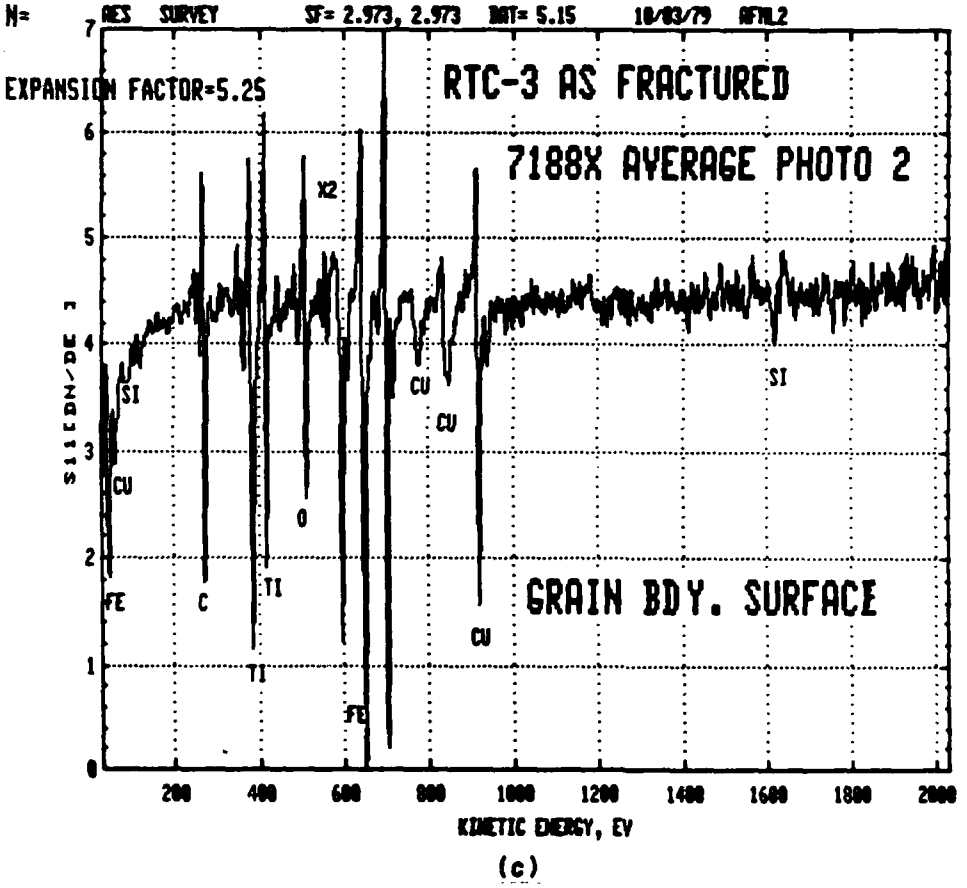

Figure 2 (Continued)

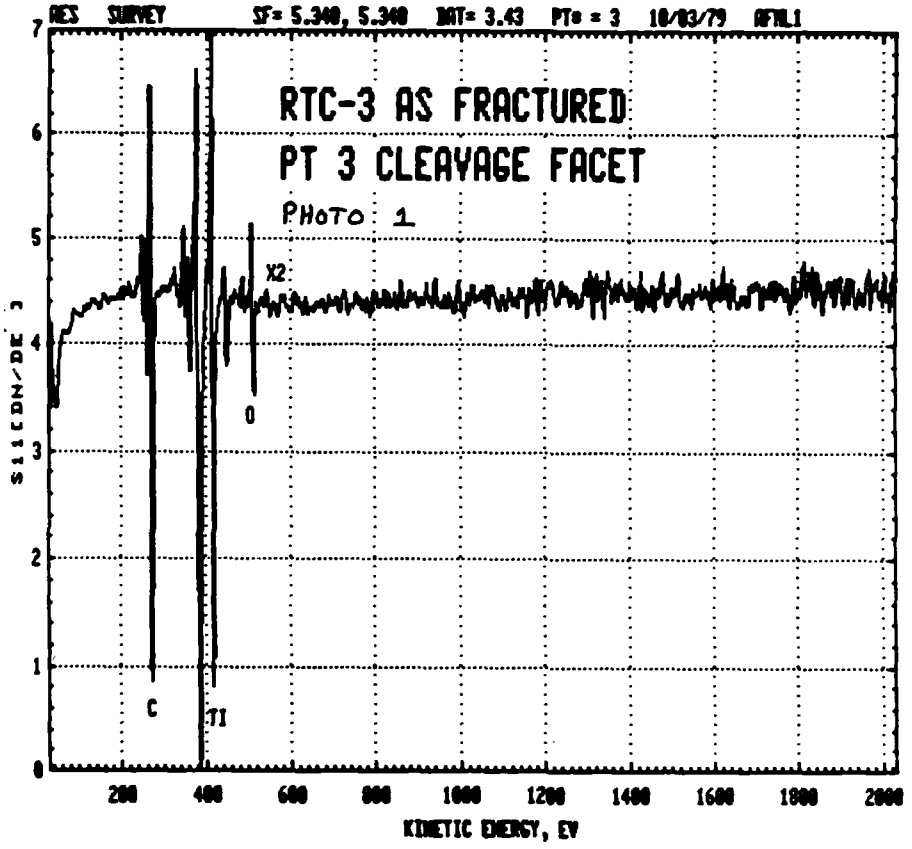

Figure 3. Auger Chemical Analysis of Cleavage Transgranular Fracture.

A series of Corning 7052 borosilicate glass - SiC composites was fabricated. The glass powder used, Corning Glass Works Code 7052, has the following physical properties:

Thermal Expansion Coefficient (α):	46×10^{-7} cm/cm/^{o}C (0 - 300^{o}C) 53×10^{-7} cm/cm/^{o}C (300^{o}C - softening point)
Density (ρ):	2.28 gm/cm^{3}
Young's Modulus (E):	8.2×10^{6} psi
Poisson's Ratio (ν):	0.22
Strain Point:	435^{o}C
Annealing Point:	480^{o}C
Softening Point:	710^{o}C
Working Point:	1115^{o}C

The SiC powders used for reinforcing purposes were 400 grit ($\cong$ 23 μm) produced by A. D. MacKay Co. The reported thermal-expansion coefficient of SiC is 47×10^{-7} cm/cm/^{o}C, and this value is very near that of the glass used and, hence, minimizes the stress build-up between glass matrix and SiC particles. The volume percentages of SiC chosen for the composites were 0, 2, 5, 10, and 20. The desired volume percent of the SiC powder was mixed with glass powder in a Spex mill/mixer with plastic balls for 30 min. This mixing procedure resulted in an intimate mixture of glass and SiC powders.

In the initial stages of the present study, it was found that during hot pressing, gases were evolved continuously from the powder mixture, presumably due to adsorbed water or gas-producing organic matter. These gases resulted in residual porosity of as much as 10%; also high-temperature hot pressing ($< 800^{o}$C) resulted in residual porosity, presumably due to the decomposition of the volatile constituents in the glass or other organic matter. Nevertheless, the optimum hot-pressing condition was established, and the desired glass - SiC composites were successfully vacuum hot pressed. The bulk densities of the five different

composites were measured, and the values matched with those of the rule-of-mixture calculation. The bend bars (1/4 × 1/8 × 1 1/2 in.) were cut from the hot-pressed disk using a diamond cutting wheel. The tensile surfaces of the bars were beveled and polished using 6-μm diamond paste. After polishing, the bend bars were annealed at 500°C in air for 1 hr. to relieve the residual stresses.

The fracture strength of the composites was measured utilizing four-point-bend testing. Figure 4 is a plot of fracture strength as a function of vol% SiC. As can be seen, a sharp drop in strength occurs with a small (2 vol%) amount of SiC particulate addition, followed by a monotonic increase in strength up to 50 vol% SiC. This initial strength drop was also observed by Hasselman and Fulrath[1] in their study of glass-Al_2O_3 systems and later discussed by Miyata and Jinno,[2] and Borom.[3] Miyata and Jinno explained, based upon their model, that at low volume fractions of the dispersed phase, macroscopic fracture occurs as a result of the growth of the micro-cracks originating in the vicinity of the pre-existing structural imperfections through a heterogeneous nucleation process; in this case, strength decreases with the proportion of the dispersed phase. At higher volume fractions where further crack propagation is prohibited by the hard crystalline particles, the process of crack propagation around the dispersed particles may be responsible for the macroscopic fracture of the composite; in this case, strength is an increasing function of the volume fraction. These two competing phenomena exhibit a minimum in a plot of strength vs vol% of the dispersed phase. Borom explained the strength increase as a function of vol% of the dispersed phase by introducing the load-sharing concept. However, the strength decrease at a low vol% of the dispersed phase was explained, although not very satisfactorily, based upon the probability of finding a particle within three particle radii of a flaw at the tensile surface where the maximum tensile stress occurs.

In any case the trend for the strength vs. vol% second-phase data in this study is similar to that for the glass-Al_2O_3 system which was studied by Hasselman and Fulrath.[1] However, the drop in strength at low vol% is

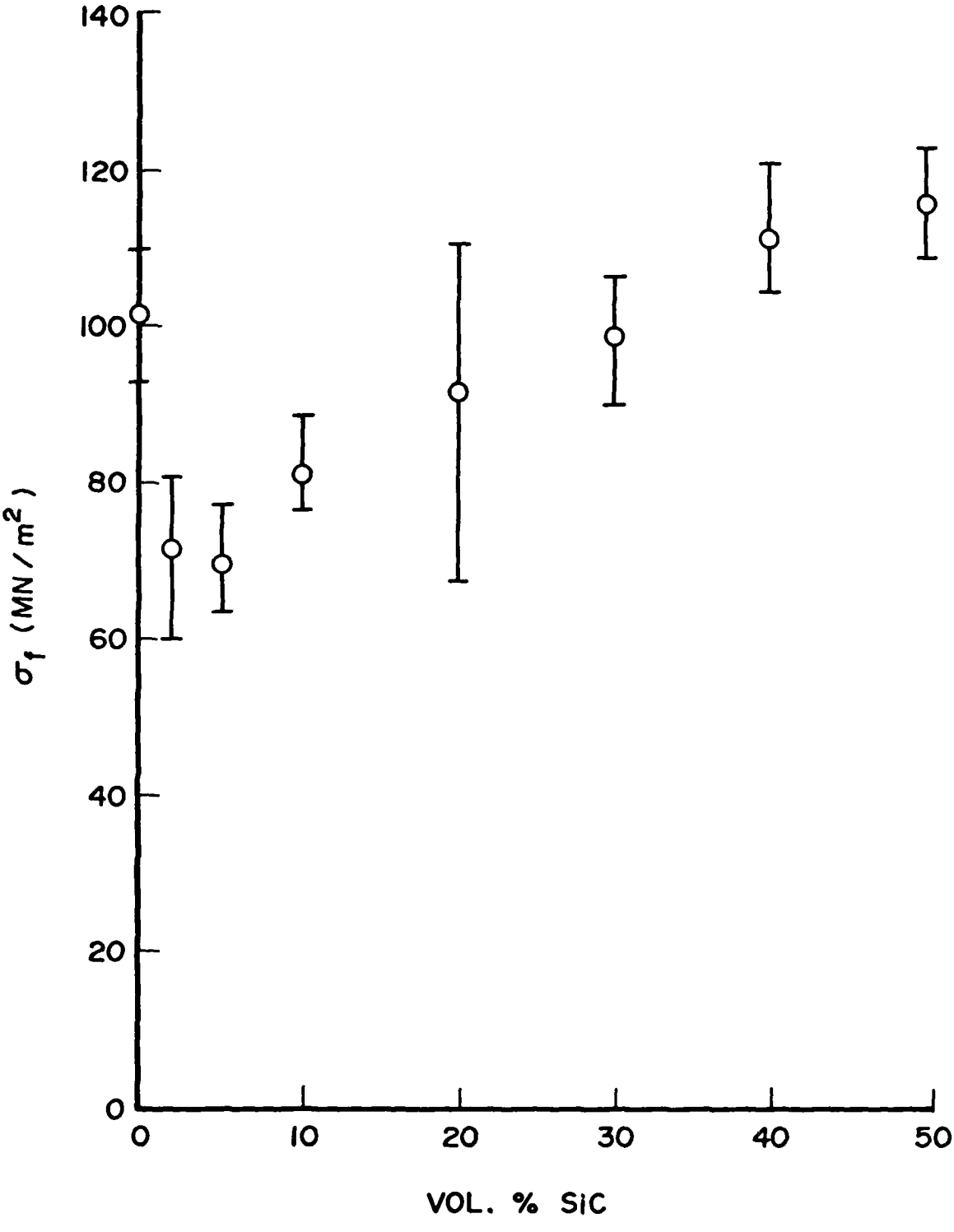

Figure 4. Fracture Strength of a Composite Series vs. vol% of SiC Dispersed Second Phase.

much steeper, and the increase in strength at higher vol% is rather gradual. These differences from the strength data of the previous glass-Al_2O_3 system may involve the effect of the following combination of factors in the glass-SiC system: residual porosity, the shape of the SiC particles (plate-like faceted shape), a small thermal-expansion mismatch ($\alpha_{glass} > \alpha_{SiC}$) causing radial matrix tensile stress around the particle), and poor interfacial bonding or wetting in glass-SiC as compared to glass-Al_2O_3. It is difficult to rank these factors; however, it is expected that the combination of these factors causes the deviation from the previous glass-Al_2O_3 investigation.

The fracture toughness of the composites was measured using the controlled-surface-indentation-flaw technique. The load used to produce a Knoop indentation was 3.1 kg, which generated a semi-circular flaw having a surface dimension of ~ 330 μm. This flaw is sufficiently large to cause an interaction of the crack front with the dispersed SiC particles. Figure 5 is a plot of K_{IC} as a function of vol% of the dispersed SiC phase. The measured K_{IC} value of the glass (≅ 0.7 Mn/m 3/2) is comparable to the reported value for Pyrex®. The K_{IC} of the composite increases linearly with vol% SiC. Lange[4] measured the fracture energy of the glass-Al_2O_3 system which is similar to the system studied by Hasselman and Fulrath.[1] He proposed that the increase in fracture energy is due to an increase in the line tension of the crack front pinned by the dispersed particles. Figure 6 shows the fracture surface of a 10 vol% SiC-glass composite in which the fracture originated at the controlled semicircular flaw. The semicircular crack front is impeded by a random array of SiC obstacles during propagation, and it bows out between them. The wedge-shaped cracks, which experienced no stress, show the crack-front pinning and breakaway positions of two crack-front segments on two sides of a particle. These observations clearly indicate that crack-front/particle interactions must contribute, in part, to the observed increase in K_{IC}.

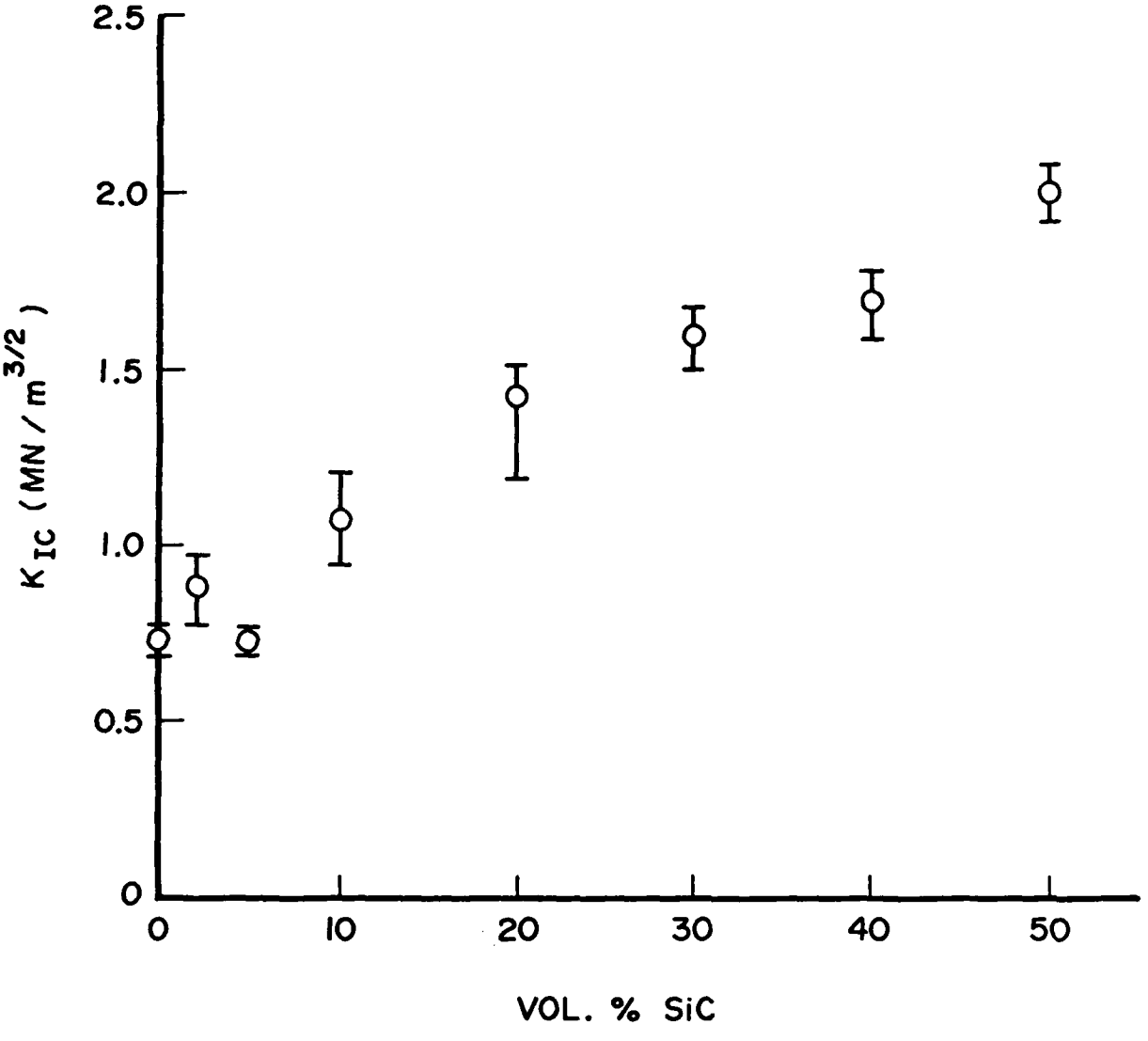

Figure 5. Fracture Toughness (K_{IC}) of a Composite Series vs. vol% of SiC Dispersed Second Phase.

Swearengen, et al.,[5] studied the fracture toughness of borosilicate glass containing dispersed Al_2O_3 spheres. They found that K_{IC} increases linearly with volume fraction of Al_2O_3 to a value three times that of the base glass at 40 vol% Al_2O_3. They also found that the toughness increases directly with composite modulus; however, the increase is greater than that which would be expected from the simplified load-sharing model.

As described above, the interpretation of the data--and thus the strengthening mechanisms of the brittle matrix - brittle particulate composite system--differs depending upon which correlating variable in the Griffith equation (i.e., flaw size, fracture energy, and Young's modulus) is considered to be dominant.

3. MONOLITHIC ALKOXY-DERIVED MULLITE

Stoichometric mullite is an excellent host matrix material for particle and/or fiber composites. It retains its orthorhombic crystal structure up to 1828 ± 10°C, where it melts incongruently.

Alkoxy-derived mullite was fabricated and characterized. Mullite powder was prepared by the hydrolytic decomposition of mixed alkoxides, followed by drying and calcining. The dense mullite disc* was prepared by hot-pressing alkoxy-derived mullite powders under 6000 psi at 1500°C for 30 min. The bend test bars (≅ 1 × 1/4 × 1/8 in.) were prepared using a low-speed diamond saw (Isomet®). Surfaces of the bend bars were polished with a 15-μm diamond disc, and the edges of the tensile surface were beveled. Test specimens were annealed at 1500°C for 0.5 hr. in air before being subjected to the final polish with 9-μm diamond paste.

Figure 7 shows the light translucency of a 0.75-mm-thick mullite specimen. As can be seen in Fig. 7(a), elongated speckles obstruct the light transmission. This feature is shown more clearly in Fig. 7(b), which is a transmission optical micrograph of the same specimen. It reveals a

*Furnished by K. S. Mazdiyasni, AFWAL/MLLM.

Figure 6. Enlarged Fracture Surface of Glass-10 vol. SiC, Showing the Interaction of the Crack Front with the Particle Obstacles.

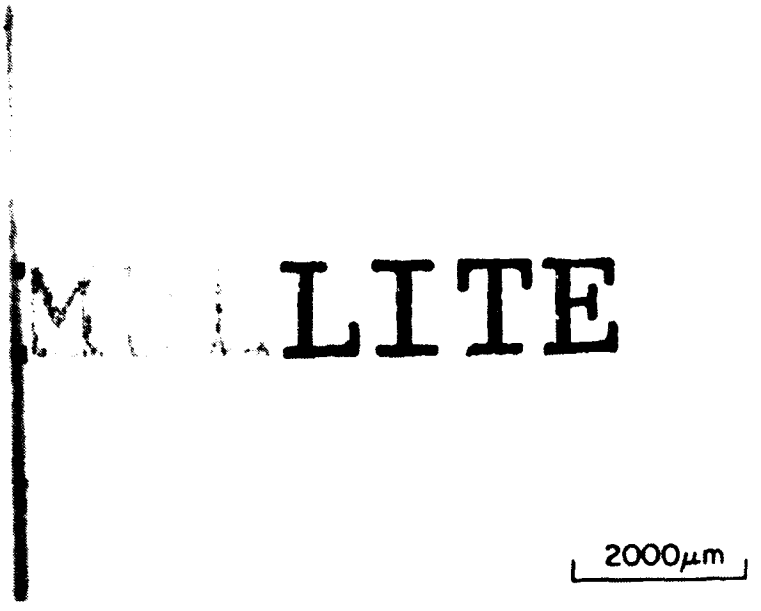

(a)

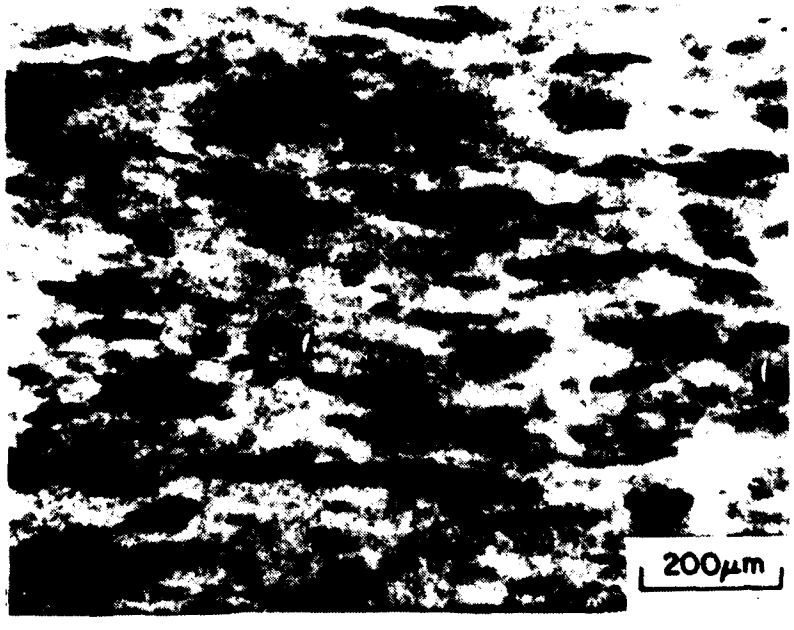

(b)

Figure 7. Translucency of Mullite as Evidenced by Letters MULLITE Showing through 0.75-mm-Thick Specimen. (a) Light transmission through Mullite specimen showing porosity nests and (b) Hot-pressing axis, vertical.

significant area distribution of porosity which appears as dark regions in the photograph. These observed "nests" of porosity are thought to be associated with the original segregated agglomerate structure of the raw material. The effects of these porosity nests upon the mechanical properties will be discussed later in conjunction with SEM fractographs. It should also be noted that the porosity-nest "pancake" lies perpendicular to the hot-pressing direction.

Figure 8 is an optical micrograph of the specimen etched with HF acid. The porosity nests are badly etched due to the interconnected pores in this region and appear to have a smaller grain size than that of the "matrix." The average grain size in the matrix is on the order of 6 μm.

Figure 9 is the four-point-bend strength of mullite plotted as a function of temperature. Average strength values based upon three tests are 18.6 kpsi at room temperature, 20.35 kpsi at 1400°C, and 21.07 kpsi at 1500°C. The increase in the fracture strength at the higher temperature can be explained as follows. The high-temperature strengthening response is due to diminution of the crack-tip stress intensity by plastic relaxation due to the grain-boundary viscous phase. Govila, et al.,[6] also observed this type of phenomenon in a lithium-alumino-silicate (LAS) glass ceramic and have explained it as incipient crack-branching or slippage along grain boundaries in proportion to the local resolved shear stress within the stress field of the crack tip.

Figure 10 shows the fracture origin of the mullite tested at room temperature. The fracture originated beneath the surface and appeared to initiate in the vicinity of the small-grained porosity nest. Figure 11 clearly shows this feature where the fracture has initiated from the porosity nest. Figure 12 is the optical micrograph of the tensile surface of the sample which was tested at 1500°C. The fracture initiated from the "boundary" of the porosity nest and the large-grained region. As can be seen in Fig. 11 (tested at 1400°C) and Fig. 13 (tested at 1500°C), a substantial amount of slow crack growth (intergranular fracture) had occurred before the specimens failed catastrophically (transgranular fracture).

(a)

(b)

Figure 8. Optical Micrograph of Polished and Etched (1.5 hr. 50° HF) Surface of Mullite (Parallel to the Hot-Pressed Direction).

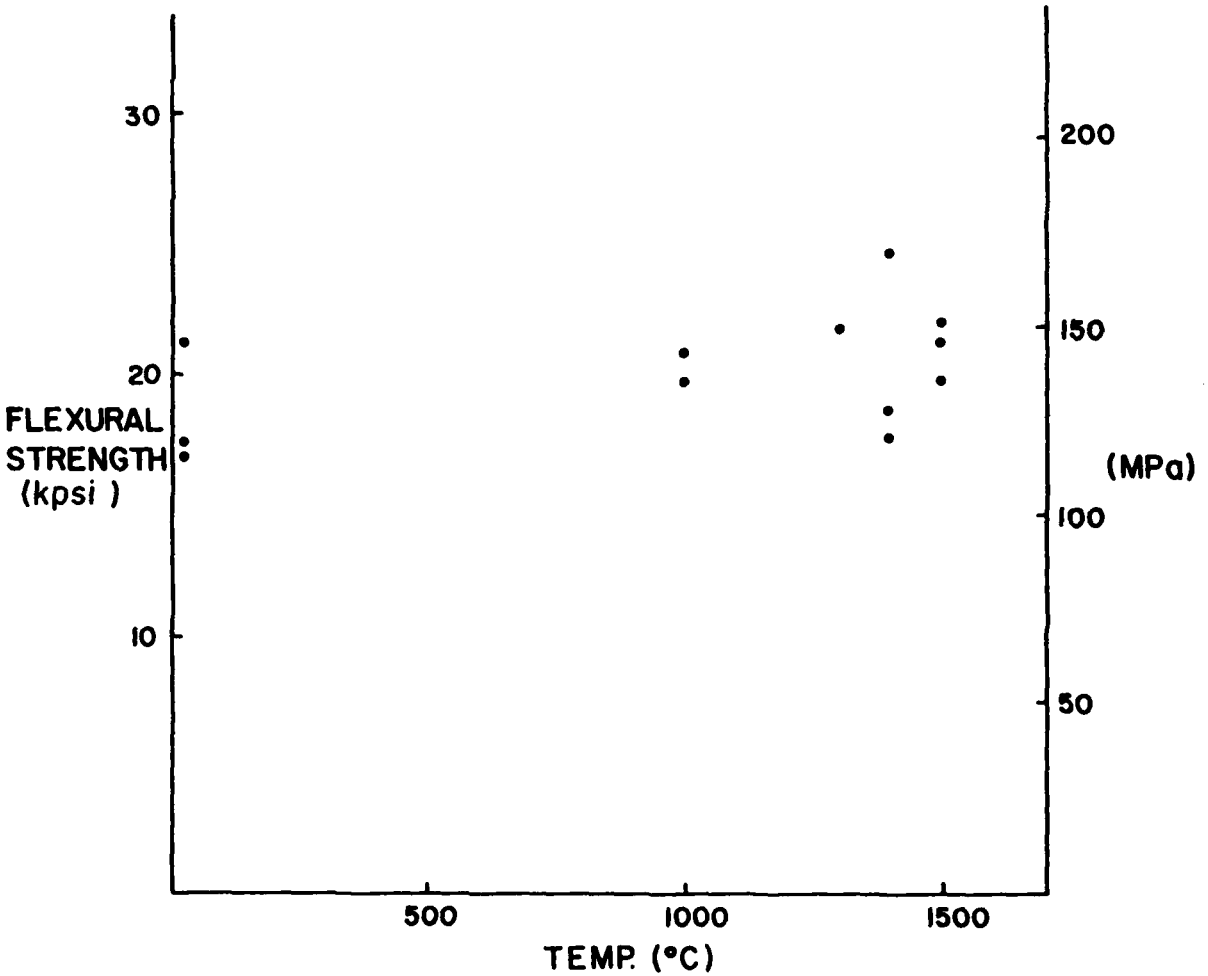

Figure 9. Plot of Flexural Strength as a Function of Temperature for Mullite.

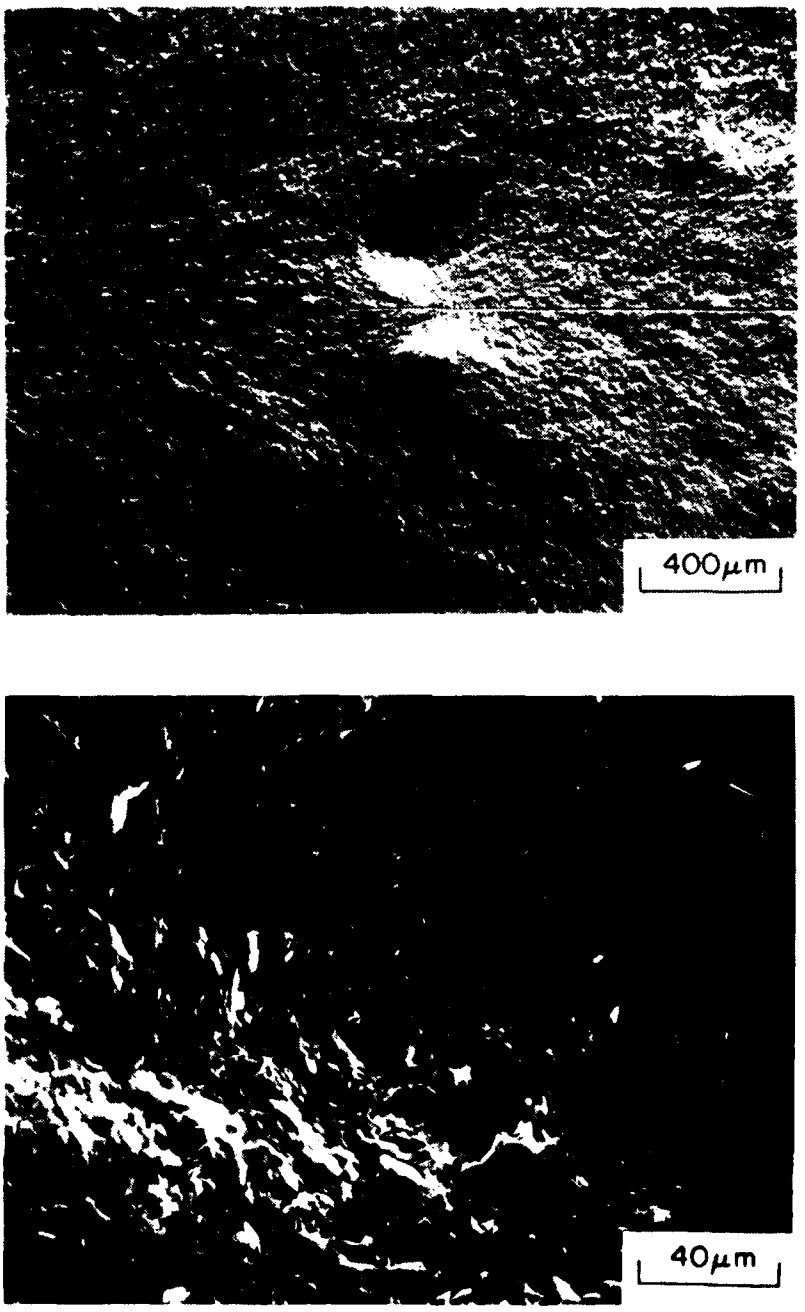

Figure 10. Fracture Surface of Mullite Tested at Room Temperature.

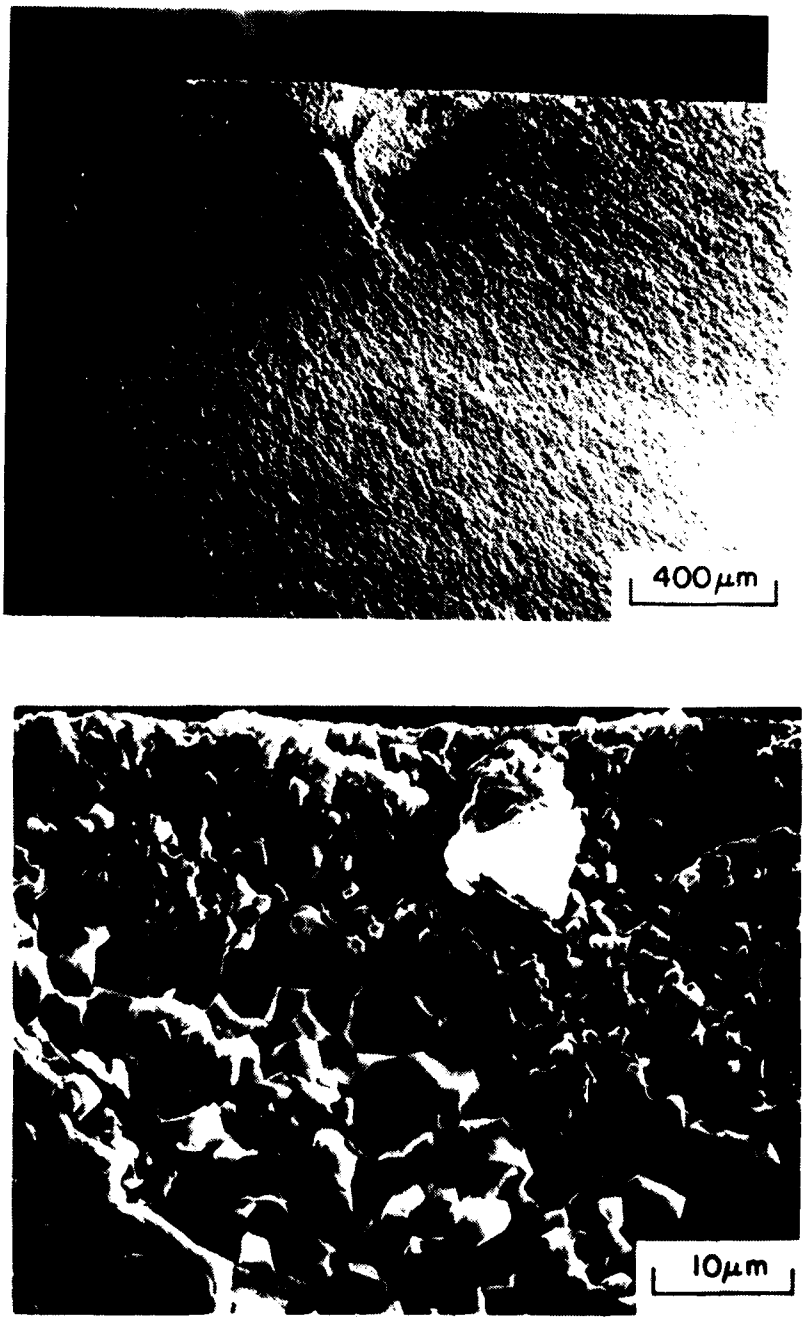

Figure 11. Fracture Surface of Mullite Tested at 1400°C.

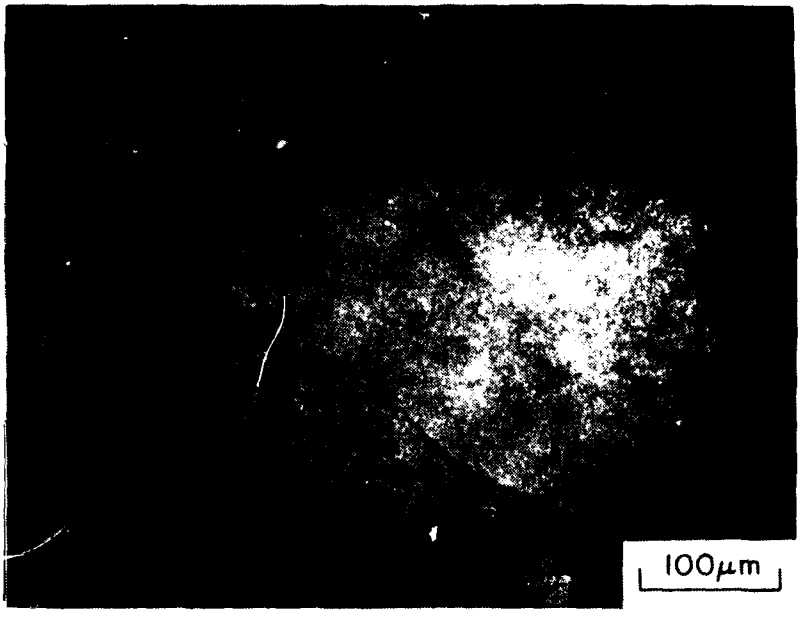

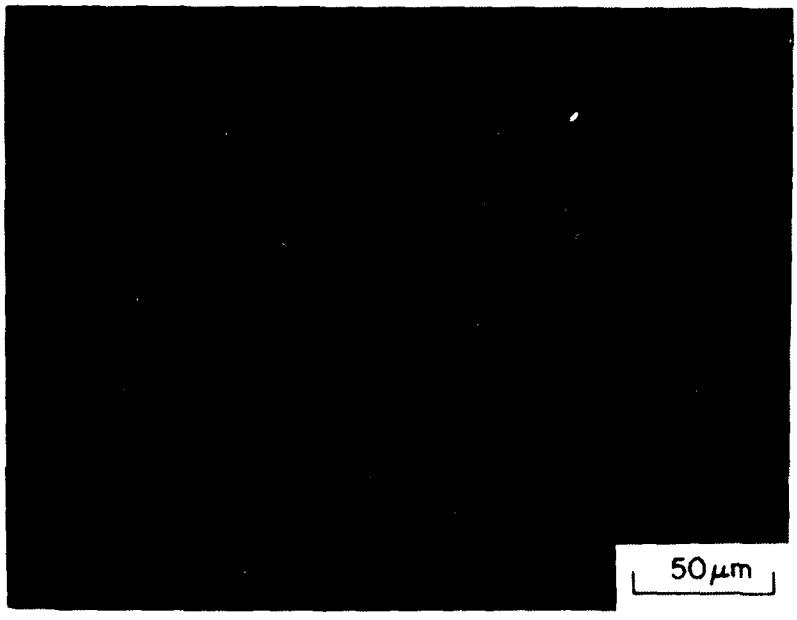

Figure 17. Optical Micrograph of Tensile Surface of Bend Bar Tested at 1500°C.

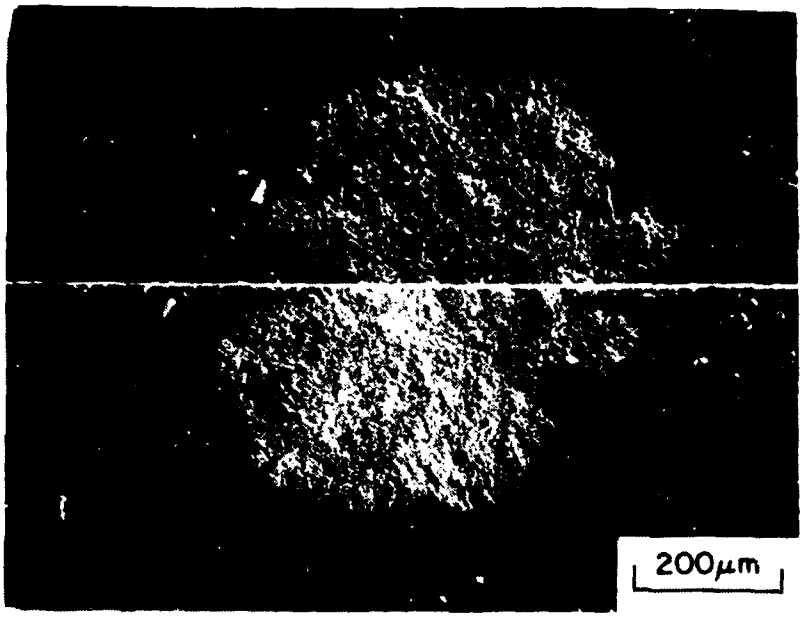

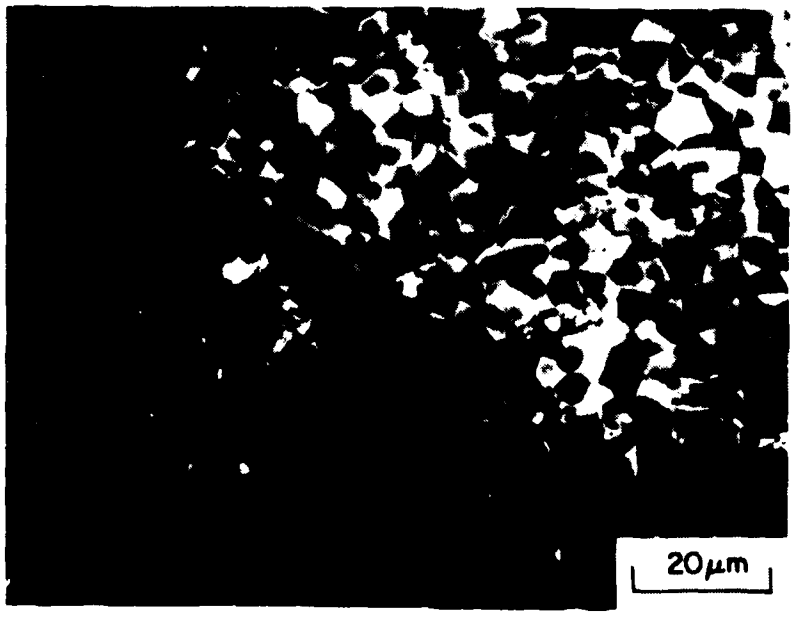

Figure 13. Fracture Surface of Mullite Tested at 1500°C.

The slow crack growth in this material was clearly verified in Fig. 14 where a 1-Kg-load Knoop diamond-indentation controlled flaw was placed on the tensile surface before the 1500°C fracture test. These results indicate that although stoichiometric mullite is utilized, a minute amount of highly viscous refractory glass phase exists in the specimen. However, the strength data up to 1500°C are encouraging since they do not show any strength degradation. It is expected that the strength of the mullite can be increased through optimization of processing conditions in such a way as to avoid the raw-material agglomeration which causes the porosity nests.

The K_{IC} of these specimens was also measured utilizing the indentation-controlled-flaw technique. At room temperature the average K_{IC} value is 1.5 $MN/m^{3/2}$; at 1500°C (based upon the flaw size from Fig. 14), the K_{IC} value was calculated to be ~ 2.5 $MN/m^{3/2}$.

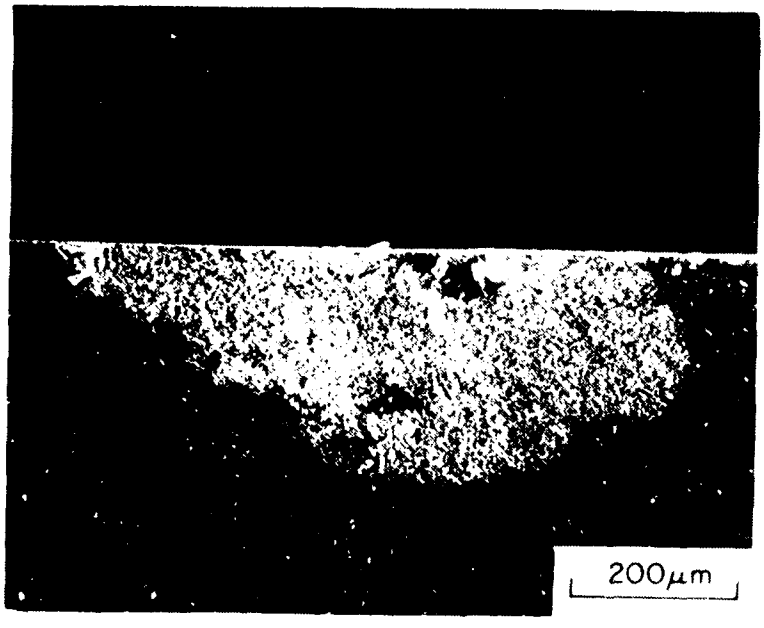

(a)

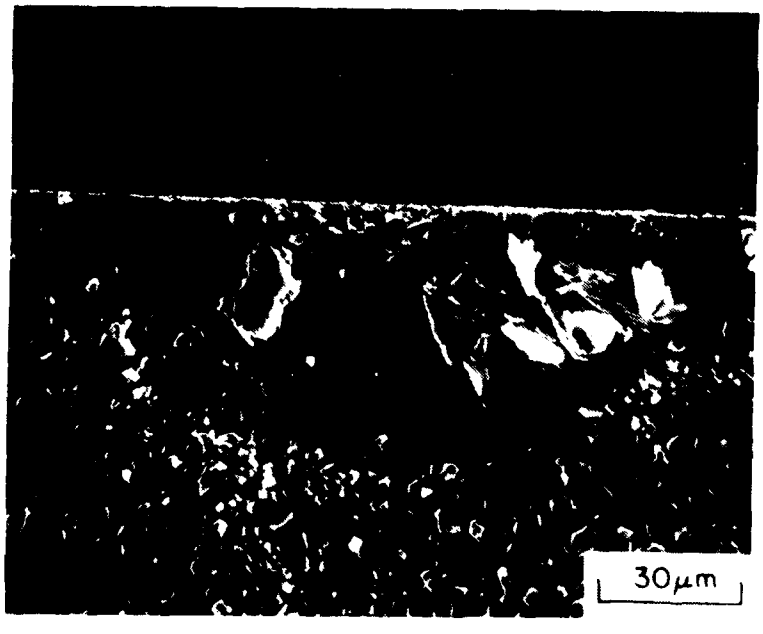

(b)

Figure 15. Fracture Surface of Mullite 1-Kg Load Knoop Diamond Indented Prior to Test at 1500°C.

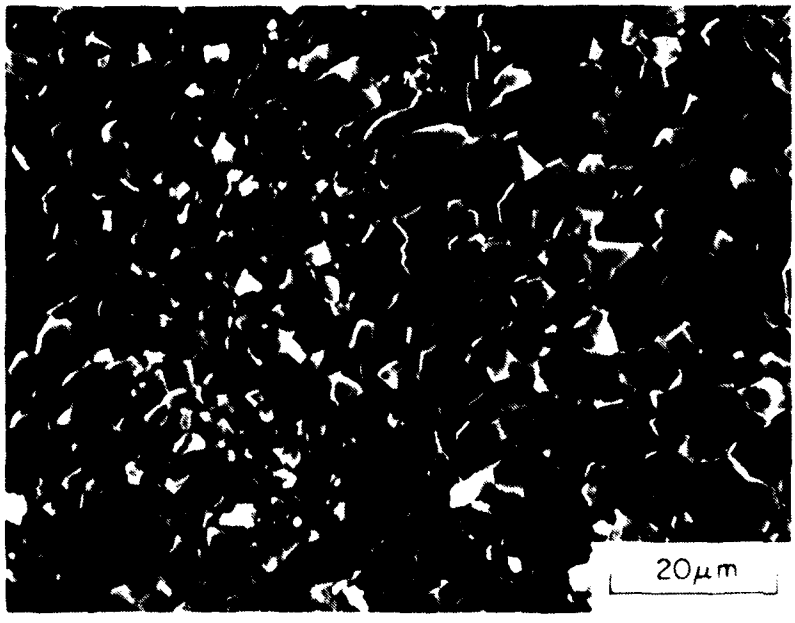

(c)

(d)

Figure 1. (Continued)

Section IV

PUBLISHED PAPERS

"Deformation Behavior of Single Crystals of Titanium Carbide," D. K. Chatterjee, M. G. Mendiratta, and H. A. Lipsitt, J. Mater. Sci. 14 (9), 2151 (1979).

"Electron Irradiation Damage in Titanium Carbide," D. K. Chatterjee and H. A. Lipsitt, J. Less Common Metals 70 (1), 111 (1980).

"Steady State Creep Behavior of Ti_3Al-Base Intermetallics," M. G. Mendiratta and H. A. Lipsitt, J. Mater. Sci. 15, 2985 (1980).

"Fracture Toughness and Strength of the Si_3N_4-TiC Composite System," T. Mah, M. G. Mendiratta, and H. A. Lipsitt, Bull. Am. Ceram. Soc. 60, 1229 (1981).

"Electron Irradiation Damage in TiC," G. Das, D. K. Chatterjee, and H. A. Lipsitt, J. Mater. Sci. 16, 3283 (1981).

"Mechanical Properties of Polycrystalline TiC," G. Das, K. S. Mazdiyasni, and H. A. Lipsitt, J. Am. Ceram. Soc. 65, 104 (1982).

"Measurement of the Stacking-Fault Energy of TiC," G. Das, J. Less Common Metals 83, L7 (1982).

Section V

RESTRICTED REPORTS TO BE PUBLISHED

"Tensile Flow and Fracture Behavior of Fe_3Al," D. K. Chatterjee, M. G. Mendiratta, S. K. Ehlers, and H. A. Lipsitt.

"Tensile Behavior of Fe-31 at% Al Alloy," S. K. Ehlers and M. G. Mendiratta.

REFERENCES

1. D. P. H. Hasselman and R. M. Fulrath, "Proposed Fracture Theory of a Dispersion-Strengthened Glass Matrix," J. Am. Ceram. Soc. 49 (2), 68 (1966).

2. N. Miyata and H. Jinno, "Theoretical Approach to the Fracture of Two-Phase Glass-Crystal Composites," J. Mater. Sci. 7, 973 (1972).

3. M. P. Borom, "Dispersion-Strengthened Glass Matrices-Glass-Ceramics, A Case in Point," J. Am. Ceram. Soc. 60 (1-2), 17 (1977).

4. F. F. Lange, "Fracture Energy and Strength Behavior of a Sodium Borosilicate Glass-Al_2O_3 Composite System," J. Am. Ceram. Soc. 54 (12), 614 (1971).

5. J. C. Swearengen, E. K. Beauchamp, and R. J. Eagan, "Fracture Toughness of Reinforced Glasses," in Fracture Mechanics of Ceramics, Vol. 4 (R. C. Bradt, D. P. H. Hasselman, and F. F. Lange, Eds.) (Plenum Press, NY, London, 1978), pp. 973-987.

6. R. Govila, K. R. Kinsman, and P. Beardmore, "Fracture Phenomenology of a Lithium-Aluminum-Silicate Glass-Ceramic," J. Mater. Sci. 13, 2081 (1978).

APPENDIX

PAPERS SUBMITTED FOR PUBLICATION

OBSERVATIONS ON THE EARLY STAGES OF OXIDATION OF TITANIUM CARBIDE*

D. K. CHATTERJEE and H. A. LIPSITT**

ABSTRACT

Thin sections of a TiC single crystal having the {100} orientation were oxidized at 900°C in four different partial pressures of oxygen, and the oxidation products were examined using transmission electron microscopy. At a higher partial pressure of oxygen, complete oxidation of TiC to TiO_2 was observed; whereas at lower partial pressures, epitaxial oxides were formed. These epitaxial regions were characterized, and the epitaxial growth relationships of these oxides with respect to the TiC matrix were established.

---

*Submitted to Metallurgical Transactions A.

**D. K. CHATTERJEE is Research Metallurgist, Systems Research Laboratories, Inc., Dayton, OH; H. A. LIPSITT is Group Leader, Processing and High Temperature Materials Branch, Air Force Wright Aeronautical Laboratories, Wright-Patterson Air Force Base, OH.

INTRODUCTION

Titanium carbide possesses the B1-type (NaCl) crystal structure and exists over a wide substoichiometric composition range while maintaining the same crystal structure. Although TiC has many attractive properties, brittleness at low temperatures and poor oxidation resistance at high temperatures tend to restrict its range of applications. Only a few high-temperature oxidation studies on TiC have been reported, and these have been summarized elsewhere.[1] These studies showed the oxidation behavior of TiC to be similar to that of Ti. Detailed analysis of the nature of TiC oxidation products and their growth relationships, particularly those products which form during the initial stages of oxidation, has been reported in the literature;[2-4] however, the results are inconclusive--presumably due to the complexity of the oxidation products.

The present paper describes observations on the early stages of oxidation of {100} surfaces of TiC single crystals exposed to varying partial pressures of oxygen. Epitaxial growth relationships of the reaction products derived from the electron-diffraction analyses and the electron microscopic observations of the nature of the oxidation products are compared with earlier published results.

EXPERIMENTAL

The samples used in this study were cut from a single-crystal boule having a C:Ti ratio of 0.93. This single-crystal boule was oriented by the standard Laue back-reflection method to obtain {100} faces and oriented {100} slices, 0.25-mm-thick, were cut from the boule. Discs, 3 mm in diam, were removed from

these slices by spark machining. These discs were electrolytically thinned using a double-jet technique in an electrolyte consisting of perchloric acid, butanol, and methanol in the ratio 1:4:10 by volume. Thinning was conducted at -20°C at ~ 20 V. These thinned specimens were examined in both a Philips EM300 and a JEOL JEM120CX TEMSCAN microscope, both before and after the specimens were oxidized. All dark-field images were taken in the centered dark-field mode.

For oxidation, the thinned specimens were wrapped in platinum foil and oxidized at 900°C in a tubular furnace equipped with both a high-vacuum system and a gas-handling system. The furnace chamber was first evacuated to 10^{-6} Torr, and the temperature was maintained at 900° $\pm$ 2°C. Depending upon the partial-pressure-of-oxygen (P_{O_2}) requirements of the experiment, either O_2 gas or a CO-1.26 pct CO_2 gas mixture was used in the gas-handling system. When the furnace environment and the temperature were stabilized, the platinum-foil-wrapped specimens were inserted into the hot zone of the furnace. The P_{O_2} used in these experiments were ~ 100, 10^{-6}, and 10^{-20} Torr; the lowest P_{O_2} of 10^{-20} Torr was achieved using a CO-1.26 pct CO_2 gas mixture at 900°C.[5] In addition, <u>in-situ</u> oxidation experiments were conducted at 900°C in the electron microscope using a heating stage. For this experiment, the P_{O_2} of the ambient environment in the microscope was estimated to be ~ 10^{-4} Torr. After each oxidation experiment, the oxidation of the specimens was characterized in the electron microscope using bright-field, dark-field, and selected-area electron-diffraction techniques. In some of the experiments, thicker specimens (0.50 mm thick and 3 mm in diam) were oxidized in order to observe the bulk oxidation effects. These specimens, after oxidation, were ground from both sides, thinned using the technique described above, and examined in the electron microscope.

RESULTS

A typical electron micrograph and the associated electron-diffraction pattern obtained from the specimens oxidized at a P_{O_2} of 100 Torr and at 900°C for 0.5 h are shown in Figs. 1(a) and (b). From the oxidation products in the micrograph, it appears that complete oxidation of TiC has occurred. The polycrystalline-ring diffraction pattern obtained from these specimens was indexed as rutile (TiO_2) which has a body-centered tetragonal (P42/mmm) structure. In this diffraction pattern, the reflections due to TiC were not observed, which confirms that the TiC had completely oxidized to form TiO_2.

The specimens which were oxidized at ~ 10^{-4} (<u>in-situ</u> heat treatment), 10^{-6}, and 10^{-20} Torr showed lath-shaped features having two orientation variants, i.e., the laths were lying at right angles to each other (Figs. 2-4). However, it can be seen from these micrographs that the population density of the laths became lower as the P_{O_2} was reduced. Selected-area diffraction patterns obtained from these specimens were complex and, as a result, the detailed features in these patterns (streaking, satellites, etc.) could not be fully interpreted. However, the diffraction spots due to TiC could be separated from some of those due to the laths by examining unoxidized TiC in the microscope. The diffraction spots from the laths could be indexed as TiO_2 (rutile). On this basis it was concluded that the laths were thin islands of epitaxial oxide. From these selected-area diffraction patterns, the epitaxial growth relationship of TiO_2 with respect to the matrix, TiC, was found to be

$$(200)_{TiC} \parallel (002)_{TiO_2}$$

$$[002]_{TiC} \parallel [200]_{TiO_2}.$$

Details of the above analysis are represented by means of the schematic in Fig. 5.

The oxidation products for the TiC heat treated at a P_{O_2} of 10^{-20} Torr were examined in more detail employing high-magnification electron microscopy. When individual laths in these foils were imaged in the dark-field mode using the TiO_2 spots in the diffraction patterns, not only were they in contrast but also anti-phase domain boundaries (APBs) and fringes within them were revealed (Fig. 6). The APB's observed in these foils appeared to be similar to those observed in TiO_2.[6] No attempt has been made to determine the plane of the APBs and their displacement vectors in part because of the complexity of the diffraction pattern resulting from the overlapping of the laths and the matrix TiC and also because of the small dimensions of the laths.

In the high-resolution dark-field mode, when the laths were imaged using the TiC matrix and the coincident TiO_2 spots, Moiré fringes were observed in the precipitates. A typical set of these Moiré fringes is shown in Fig. 7. This micrograph was taken using the (002) TiC matrix spot, and the spacing of the Moiré fringes is D_m (measured) = 48.7 Å. This spacing does not correspond to the calculated value of Moiré fringes which would be produced for TiO_2 on TiC. However, the calculated value for Moiré fringe spacing, made on the assumption* that the (002) plane of TiO is parallel to the (002) plane of TiC,

*Lattice parameter of stoichiometric TiO = 4.17 Å and $TiO_{d_{002}}$ = 2.085 Å

Lattice parameter of TiC = 4.3285 Å and $TiC_{d_{002}}$ = 2.179 Å.

yielded D_m (calculated) = 48 Å. Since the calculated and measured values of the Moiré fringe spacings for TiO on TiC are nearly equal, it is reasonable to conclude that these laths contain disordered TiO along with TiO_2. Disordered TiO and TiC have a similar lattice structure with very similar lattice parameters.[7] Under this condition, the matrix TiC spots and spots due to TiO in the electron-diffraction pattern would coincide; and since there is very little mismatch, the epitaxial-growth relationship would be expected to be

$$(002)_{TiC} \parallel (002)_{TiO}$$

$$[002]_{TiC} \parallel [002]_{TiO}$$

The equality of the calculated and the measured Moiré fringe spacings confirms the above-mentioned growth-orientation relationship between TiC and TiO. The coexistence of TiO and TiO_2 in the early stages of oxidation of TiC is not surprising since TiO might be expected to form at lower oxidizing potentials such as a P_{O_2} of 10^{-20} Torr. Neither is it surprising that this lower oxide is partially converted t the more stable TiO_2 as the oxide film thickness increases.

For thicker specimens (0.50 mm), no precipitates were revealed when the specimens were oxidized at 900°C in a CO-1.26 pct CO_2 gas mixture, ground from both sides, and electrolytically thinned for electron microscopy. Even longer oxidizing treatments (maximum time = 75 h) produced no oxide precipitates in the bulk of the TiC specimens. In this experiment, it was thought that oxygen might diffuse through the grain boundaries and that oxides might be precipitated on the grain boundaries. Figure 8 is a typical microstructure for such a specimen; it shows that no oxides are present either within the grains or at the grain boundaries.

DISCUSSION

In the initial stage of the oxidation of TiC at 900°C, it is expected that a layer of TiO will form on the specimens of TiC and that as the oxidation continues, the TiO is likely to be converted to TiO_2. Oxidation experiments performed at 900°C for 0.5 h at 100 mm oxygen pressure produced complete oxidation of TiC, and the electron-diffraction pattern confirmed that the oxidation product is stoichiometric rutile having a tetragonal structure. In view of the very thin TiC specimens (0.25 mm) used in this study, the observation of complete oxidation of TiC to TiO_2 at 900°C in 0.5 h in the oxygen environment at a P_{O_2} of 100 is to be expected.

When the oxidation experiments were carried out at lower P_{O_2} (i.e., 10^{-4}, 10^{-6}, and 10^{-20} Torr) for the same temperature and time, the oxidation product was a mixture of TiO_2 and TiO phases. The coexistence of TiO_2 and TiO phases is expected from the point of view of a limited supply of oxygen in the oxidizing environment; in this case complete transformation of TiO to TiO_2 is not possible. The existence of transition regions in epitaxially grown films is not uncommon; and of the many possible factors, a change in partial pressure of the reactant gas may be a contributing factor.[8] The presence of TiO in the oxidation products (i.e., lath-shaped precipitates) could not be established from the electron-diffraction patterns because of the identical lattice structure of TiC and TiO and the close proximity of the lattice parameters. Under this circumstance, the diffraction spots due to TiO and TiC would coincide. However, high-resolution dark-field microscopy using the (002) TiC spot revealed Moiré

fringes in the precipitates (Fig. 7), and fringe-spacing measurements corresponded to $(002)_{TiC} \parallel (002)_{TiO}$. Hollox and Smallman[4] indicated a similar epitaxial-growth relationship between TiC and TiO, although they provided no experimental evidence for the existence of TiO.

Some of the diffraction spots in the diffraction patterns obtained from these precipitates could easily be indexed in terms of TiO_2 (Fig. 5); however, the origin of other satellite spots and streaks has not been established. These spots may be due to the two different orientation variants of the precipitates, to double diffraction effects, or to both. The streaking may be due to non-stoichiometric planar defects.[4] These precipitates clearly show characteristic APB's as seen by Van Landuyt, et al.,[6] in rutile (TiO_2).

The epitaxial-growth-orientation relationship established in this study is not in conformity with those established by Ashbee and Smallman,[3] Ashbee and Eeles,[2] and Hollox and Smallman.[4] In the present investigation the diffraction pattern due to the oxidation products (i.e., TiO_2) is a cross-grating pattern having square symmetry. This pattern is consistent with the $(002)_{TiO_2}$-type zone axis and not the $(110)_{TiO_2}$-type zone axis as indexed by Ashbee and Smallman[3] and by Hollox and Smallman.[4] The reasons for such differences are unclear at present. The absence of characteristic oxidation products in the bulk of the thicker samples clearly indicates that at a low P_{O_2}, oxidation occurs only at the surface of the TiC specimens.

SUMMARY

At a higher P_{O_2} (~ 100 Torr), thin samples of single-crystal TiC are completely oxidized to TiO_2. However, if the P_{O_2} is lowered in the oxidizing environment, epitaxial growth of oxide precipitates is observed on the surfaces of the TiC specimens. These oxide precipitates consist of both TiO and TiO_2, and their growth-orientation relationship with TiC has been established as

$$(002)_{TiC} \parallel (002)_{TiO};\ [002]_{TiC} \parallel [002]_{TiO}$$

and

$$(200)_{TiC} \parallel (002)_{TiO_2};\ [002]_{TiC} \parallel [200]_{TiO_2}$$

At a lower P_{O_2}, bulk oxidation was not noticeable.

ACKNOWLEDGEMENTS

The authors would like to thank Prof. J. C. Williams of Carnegie-Mellon University for stimulating discussions, electron-microscopy efforts, and also critical reading of the manuscript. Thanks are also due to Dr. J. D. Venables of Martin Marietta Laboratories, who provided the TiC used in this study.

This research was supported in part under Air Force Contract F33615-78-C-5037.

REFERENCES

1. E. K. Storms: The Refractory Carbides, Academic Press, New York, NY, 1967.

2. K. H. G. Ashbee and W. T. Eeles: Acta Cryst., 1962, vol. 15, p. 1312.

3. K. H. G. Ashbee and R. E. Smallman: Phil. Mag., 1962, vol. 7, p. 1933.

4. G. E. Hollox and R. E. Smallman: Phil. Mag., 1966, vol. 13, p. 1.

5. H. C. Graham: AFWAL/MLLM, Wright-Patterson Air Force Base, Ohio, private communication, 1978.

6. J. Van Landuyt, R. Gevers, and S. Amelinckx: Phys. Stat. Sol., 1964, vol. 7, p. 307.

7. A. D. McQuillan and M. K. McQuillan: Titanium, Butterworths, Wolburn, MA, 1956.

8. L. N. Aleksandrov: J. Cryst. Growth, 1975, vol. 31, p. 103.

FIGURE CAPTIONS

Figure 1. Micrograph showing oxidation product at P_{O_2} = 100 Torr. The associated electron-diffraction pattern confirms that the oxidation product is rutile (TiO_2).

Figure 2. Oxidation product of in-situ heat treatment (P_{O_2} estimated to be ~ 10^{-4} Torr); the associated electron diffraction pattern features streaking and satellites.

Figure 3. Micrograph and electron-diffraction pattern from sample oxidized at $P_{O_2} = 10^{-6}$ Torr.

Figure 4. Micrograph and electron-diffraction pattern from sample oxidized at $P_{O_2} = 10^{-20}$ Torr.

Figure 5. Schematic illustration of diffraction patterns in Figs. 2-4, showing the indexing of reflections.

Figure 6. Micrograph obtained in high-resolution dark-field mode from sample oxidized at $P_{O_2} = 10^{-20}$ Torr using the reflection marked with the aparture.

Figure 7. Micrograph obtained in high-resolution dark-field mode from sample oxidized at $P_{O_2} = 10^{-20}$ Torr using (002) TiC matrix reflections.

Figure 8. Micrograph obtained from thick (0.5 mm) TiC Sample oxidized at $P_{O_2} = 10^{-20}$ Torr at 900°C for 75 h.

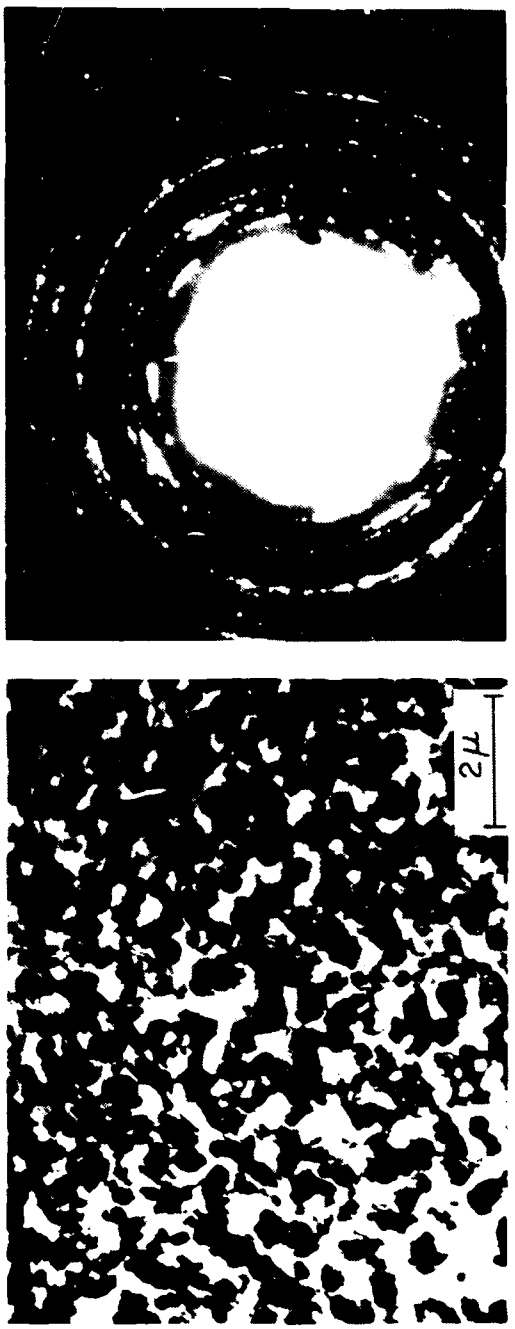

Figure 1

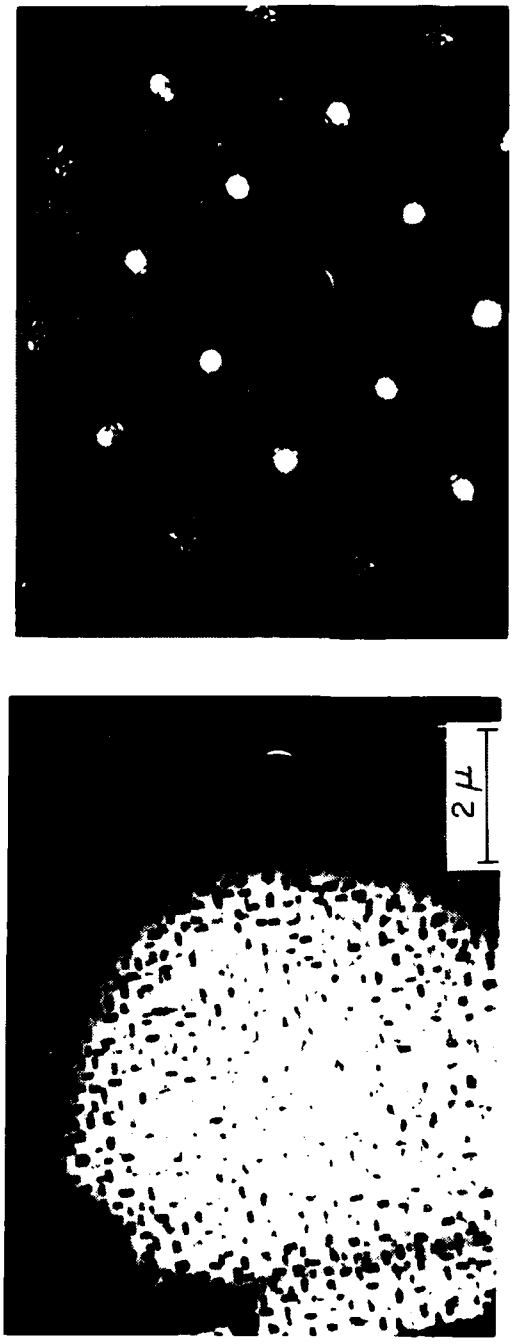

Figure 2

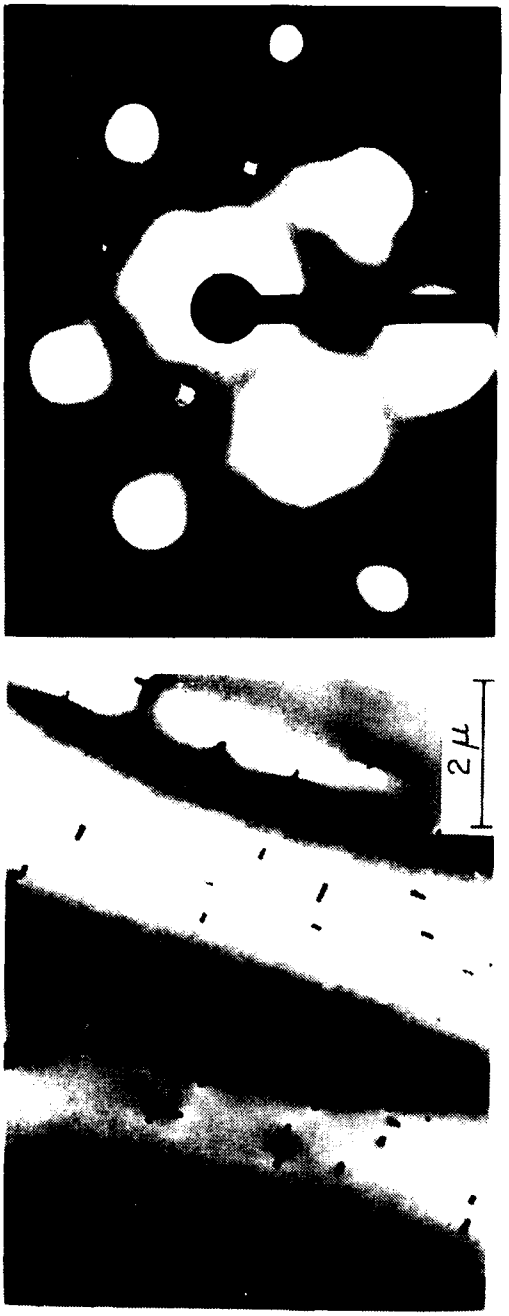

Figure 3

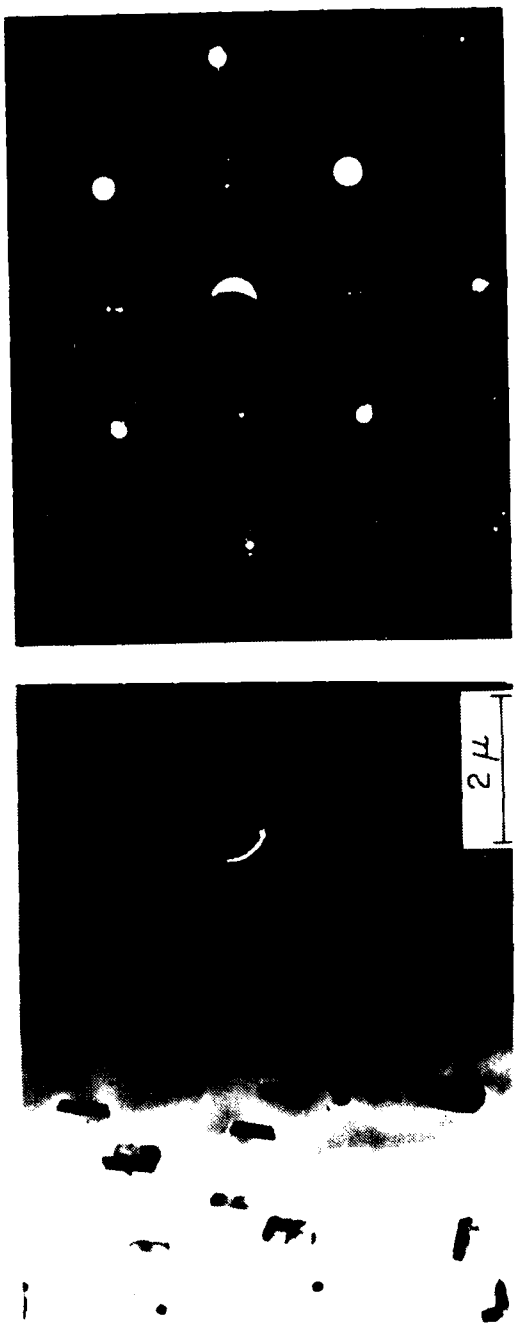

Figure 4

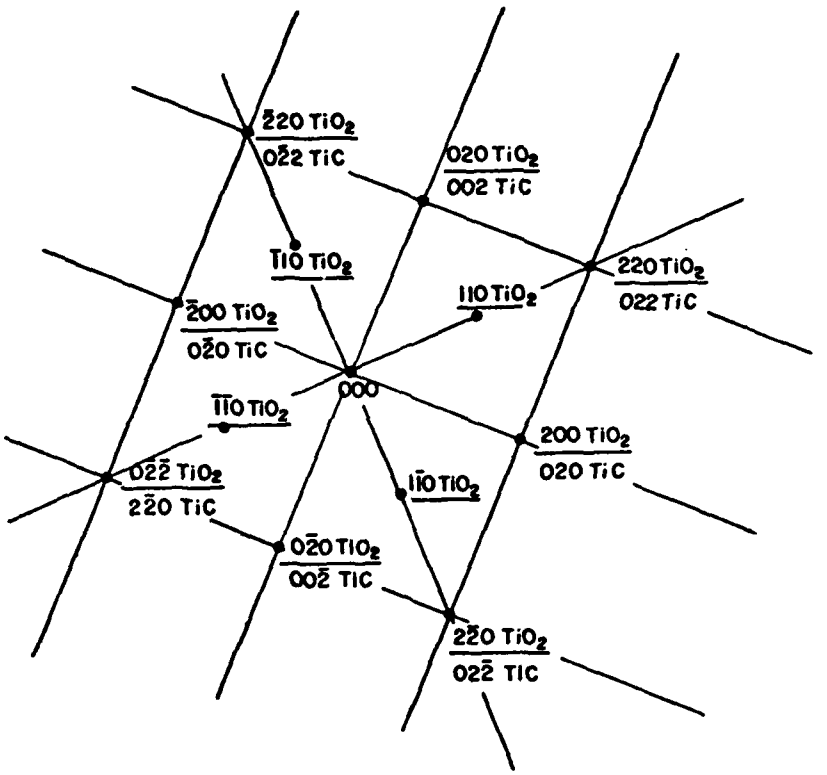
$\frac{\bar{2}20\ TiO_2}{02\bar{2}\ TiC}$
$\frac{020\ TiO_2}{002\ TiC}$
$\frac{\bar{1}10\ TiO_2}{}$
$\frac{220\ TiO_2}{022\ TiC}$
$\frac{\bar{2}00\ TiO_2}{0\bar{2}0\ TiC}$
$\frac{110\ TiO_2}{}$
000
$\frac{\bar{1}\bar{1}0\ TiO_2}{}$
$\frac{200\ TiO_2}{020\ TiC}$
$\frac{02\bar{2}\ TiO_2}{2\bar{2}0\ TiC}$
$\frac{1\bar{1}0\ TiO_2}{}$
$\frac{0\bar{2}0\ TiO_2}{00\bar{2}\ TiC}$
$\frac{2\bar{2}0\ TiO_2}{02\bar{2}\ TiC}$

Figure 5

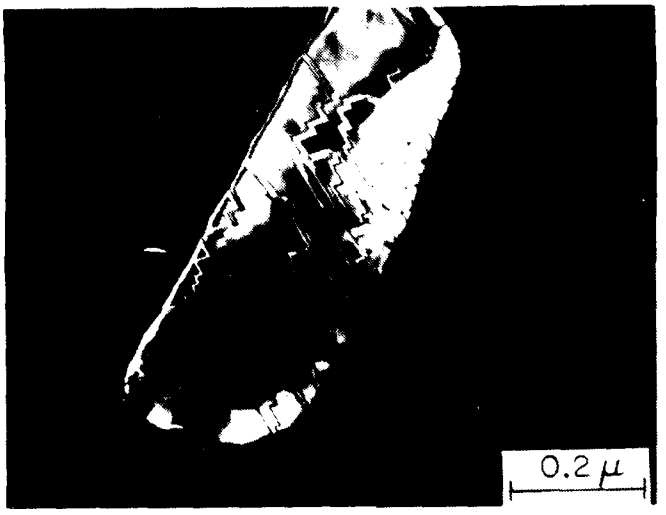

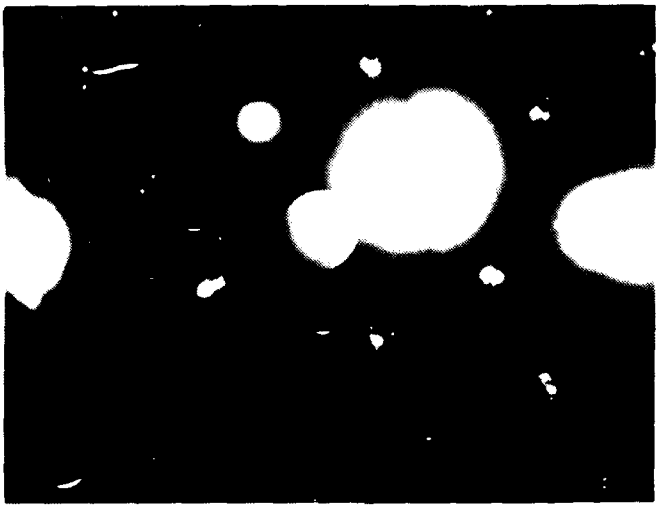

Figure 6

Figure 7

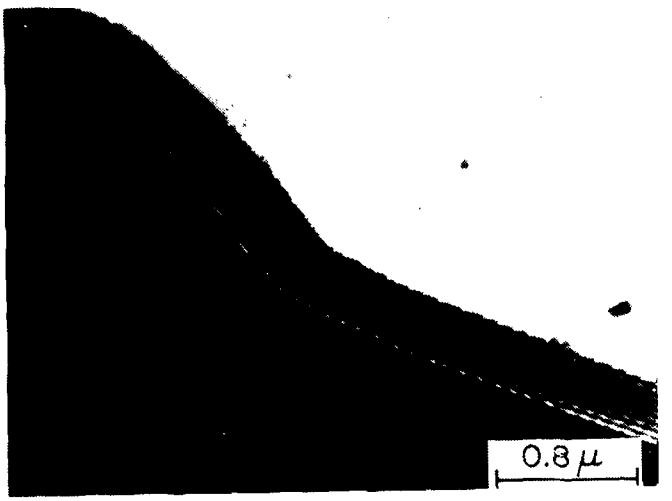

Figure 8

MECHANICAL BEHAVIOR OF POLYCRYSTALLINE TiC*

T. Mah and M. G. Mendiratta
Systems Research Laboratories, Inc.
Dayton, Ohio 45440

A. P. Katz and H. A. Lipsitt
AFWAL Materials Laboratory
Wright-Patterson Air Force Base, Ohio 45433

1. INTRODUCTION

TiC is a material of scientific interest and practical utility. It is extremely hard and has a very high melting point along with a wide range of carbon substoichiometry. The crystal structure of TiC is the rock-salt (B1) type; but, unlike many other such materials, it slips at high temperature ($\simeq$ 800°C) on {111} planes in <110> directions [1, 2]. Recent work [3] on single-crystal TiC shows that the slip system undergoes a change from {110} <110> to {111} <110> around 800°C. The importance of the {111} <110> slip is the availability of five independent slip systems, the minimum number required for a polycrystalline aggregate to deform in such a manner that the deformation in one grain is compatible with that in neighboring grains. The operation of {111} <110> slip in TiC around 800°C accounts for the transition from brittle to ductile behavior.

Few investigations have been conducted on the plastic behavior of polycrystalline TiC. Creep of fused, large-grained (1.5 × 0.3 × 0.3 mm) polycrystalline TiC above 1600°C has been studied [4]; and the bending behavior of a coarse-grained hot-pressed material has been examined up to 2070°C [5]. In addition, the mechanical behavior in compression was reported for polycrystalline TiC prepared by arc melting, r.f. melting,

*Submitted to the Journal of Materials Science

and sintering [6]. However, these results were largely nonreproducible, due in part to the difficulties in obtaining near theoretically dense polycrystalline TiC. More recently, work in this laboratory [7] on well-characterized, dense TiC showed that a ductile-to-brittle (D-B) transition at 800°C could be demonstrated for polycrystalline material in compression. No plasticity was reported in the limited bend testing performed as part of this study.

The present research was undertaken to study in greater detail the mechanical behavior in bending of high-density TiC prepared by conventional hot pressing of commercially available powders from a number of powder sources. Four-point bend testing was utilized over the temperature range 20 to 1700°C. Limited compression testing was also undertaken. During the course of this study, it was found that powder impurities played a major role in determining mechanical behavior. The effects of impurities and of heat treatments to remove those impurities were studied comprehensively, and the results were correlated with the D-B transition in polycrystalline TiC.

2. EXPERIMENTAL PROCEDURE

2.1 Materials

Nominally stoichiometric TiC powders were purchased from three commercial vendors.* The impurity contents of the powders are indicated in Table. I.

---

* (1) Hermann C. Starck, Inc., 280 Park Avenue, New York, NY 10017 (2) Refractory Metals Inc., 8450 Lockheed, Houston, TX 77034, (3) Alpha Products Ventron Division, 152 Andover St., Danvers, MA 01923.

Metallic constituent levels were determined by emission spectrographic analysis. The oxygen content was measured by neutron activation. The powders also contained free carbon as shown in the table. These analyses were carried out by placing each powder in hot aquaregia, which dissolves TiC but no free carbon. The carbon residue was collected by filtration, and the content was determined by combustion.

Powder particle-size distributions were determined by the x-ray sedimentation technique. All three lots exhibited a wide distribution. The Starck material had a maximum particle size of $\simeq$ 30 μm, median size of $\simeq$ 7 μm, and contained $\simeq$ 7% submicron fines. The RMI and Ventron powders were noticeably more coarse. The distributions ranged from $\simeq$ 40 to $\simeq$ 1 μm, with median sizes of $\simeq$ 10 and $\simeq$ 12 μm, respectively. In addition, submicron fines were essentially absent in both powders, and large particles of up to 100 μm were found in the RMI powder.

2.2 Sample Preparation

As-received and as-sieved (-400 mesh) powders were conventionally hot pressed in 2-in.-I.D. graphite dies lined with graphite foil. Pressing temperatures ranged from 1700 to 1750°C, times from 30 to 60 min., and pressures from 34 MN/m^2 (5 ksi) to 59 MN/m^2 (8.6 ksi). Consolidation was performed in vacuum (10^{-1} Torr) or argon (5 psi).

Four-point bend test specimens were diamond-saw cut from the TiC billets to the dimensions 4.5 × 2 × 26 mm. The tensile surface of each bar was

polished to 6 μm and the edges were slightly rounded to eliminate chipping. Some of the bars were subjected to a vacuum heat treatment of 2150°C for 10 hr. This was accomplished by placing the bars in tents of graphite foil located within a graphite crucible. The crucible was inductively heated to temperature and maintained under a 2×10^{-1} Torr vacuum. These bars were repolished prior to testing.

A few compression tests were conducted with heat-treated material. Specimen dimensions were 2.3 × 2.3 × 5 mm.

2.3 Test Procedure

Four-point bend tests were performed using an Instron universal test machine at a cross-head speed of 5.08×10^{-2} cm/min. (0.002 in./min.). Specimens were mounted in a SiC bending jig having an outer span of 19.05 mm (3/4 in.) and an inner span of 9.53 mm (3/8 in). Compression tests were conducted in the Instron at the same cross-head speed. The specimens were placed between two SiC platens during those tests.

The Instron was equipped with a vacuum furnace utilizing a tungsten mesh heating element for high-temperature testing in vacuum ($\simeq 10^{-4}$ Torr) or inert atmosphere. Specimens were held at temperature for ≃ 15 min. prior to testing.

3. RESULTS AND DISCUSSION

Figure 1 is an optical micrograph of a hot-pressed compact consolidated from unsieved Starck powder. This billet (designation STC-19) was pressed at 1750°C for 30 min. in vacuum with a ram pressure of 55 MN/m^2 (8 ksi). The average grain size was 12 μm; and the density, as determined by water immersion, was 4.81 g/cc (98% of theoretical based on stoichiometric TiC with lattice parameter a = 4.3285 Å). The unsieved RMI and Ventron powders did not consolidate so well, with final densities in the range 93-96% of theoretical. This is presumed to be a result of the coarser powder-size distribution and the lack of submicron fines in these starting materials. It was found that density increased with increasing ram pressure, temperature, and time over the ranges reported. There were no apparent differences in microstructures or properties when specimens pressed in vacuum were compared with those pressed in argon.

The densities of the powder compacts could be improved by sieving the as-received powders to -400 mesh. However, this introduced ≈ 300 ppm copper from the sieves which proved to be extremely detrimental to the high-temperature mechanical properties, which will be discussed later.

Figure 2 shows bend strength as a function of temperature for specimens cut from Starck billet STC-19. The room-temperature strength was maintained up to 1000°C, but a drastic drop in strength occurred at higher temperatures. For the RMI and Ventron billets pressed from unsieved powders, the low-temperature bend strength was reduced to 275 - 345 MN/m^2 (40 - 50 ksi) as a result of the extensive porosity in these billets (including pore coalescence). However, similar to the Starck billet, room-

temperature strength was initially maintained as the test temperature was raised, but dropped sharply at high temperatures. Unlike the Starck material, the strength degradation began above 800°C.

As reported, higher densities could be achieved by sieving the powders before hot pressing. This led to some increases in low-temperature strength, especially for the RMI and Ventron materials, 380 - 450 MN/m^2 (55 - 65 ksi). However, the high-temperature strength degradation for specimens fabricated from sieved powders from all three vendors began above 600°C.

Figure 3 is an SEM micrograph of the fracture surface of an STC-19 specimen tested at room temperature. The fracture mode is predominantly transgranular cleavage. Figure 4 is the corresponding fractograph for a specimen tested at 1100°C. Here the fracture is much more intergranular and continues to increase as test temperature is raised. At 1400°C the fracture is almost exclusively intergranular. In all cases the load-versus-deflection behavior is linear and the specimens fail in a brittle manner.

The fracture behavior just described holds equally well for the other materials fabricated and tested, the only difference being the temperature at which the strength begins to degrade and the failure mode begins to change.

These fracture characteristics indicate that the grain boundaries are weak at high temperatures (above 600°C for the sieved powders, above 800°C for the unsieved RMI and Ventron powders, and above 1000°C for the unsieved Starck powder). The reason for this becomes apparent when the fracture surfaces are examined more closely. Figure 5 is a higher-magnification fractograph of the 1100°C STC-19 specimen. A grain-boundary segregant can clearly be seen on the boundary facets. Veins of this segregant also line the multigrain junctions. Some of this material has melted or softened at 1100°C and "balled up" upon exposure of this free surface at fracture. The presence of a grain-boundary segregant is confirmed in the TEM. Figure 6 shows a film of the segregant separating the two grains.

Spot-mode EDX data obtained in both the STEM and SEM indicate that the segregant contains Co, Fe, and Si in the case of Starck powder compacts. A typical spectrum is shown in Fig. 7. The Ti peaks are the result of the beam-activation volume encompassing some of the TiC matrix. For RMI and Ventron powder compacts, the EDX analyses indicate the presence of Fe and Si in the segregant. When the powders are sieved, Cu joins the other elements at the grain boundaries.

In-situ Auger fracture-surface analyses confirm these results. Figure 8 is a spot-mode grain-boundary-segregant Auger spectrum from a compact fabricated from sieved RMI powder. The elemental distribution is non-uniform, since changing the Auger spot location--sometimes even within

the segregant on the same boundary--will cause a change in the relative peak intensities. The presence in the spectrum of Ti and C peaks, whose shapes and relative intensities are characteristic of TiC, was typical and resulted from beam spreading beyond the edges of the segregant patches examined and/or holes in the patches. These patches were ≈ 1 - 4 μm in diam. At the beam currents utilized to obtain good Auger signal-to-noise ratios, the effective beam diameter may have been as large as 4 - 5 μm. Furthermore, exact centering of the beam on the patch was difficult. In addition, although these layers appear to be largely continuous, the possibility of holes or discontinuities extending to the underlying grain cannot be ruled out. The conclusion that the TiC Auger peaks originated from the surface of the exposed matrix is further supported by TEM microdiffraction analyses of the grain-boundary films. No evidence was found of any TiC in the segregant.

The metallic impurities at the boundaries are not soluble in the TiC matrix. This was demonstrated by sputtering the fracture surface in the Auger, as seen in Fig. 9. Peak intensities for the major impurities change little until the interface with the underlying TiC grain is reached. At this point the peaks drop precipitously to undetectable levels. Unsputtered cleavage facets show no Fe, Co, Cu, or Si.

There is no evidence of oxygen segregation in the as-hot-pressed materials. Auger oxygen peaks of relatively low intensity are detected on the grain boundaries and cleavage facets of the in-situ fractured specimens. They are of equal intensity for all topographical areas and, since they are rapidly reduced by sputtering, are likely the result of adsorbed oxygen. These results indicate that the oxygen in the material is uniformly dissolved in the TiC matrix.

The high-temperature mechanical behavior of the hot-pressed materials can be explained by the melting and/or softening of regions of the grain-boundary segregant at elevated temperatures. If this be the case, the chemistries at the boundaries must be such that phases are formed which melt near the temperatures at which the strengths decrease. In the case of the sieved-powder compacts, this temperature was ≃ 600°C. The metallic impurities were Fe, Cu, and Si for the RMI and Ventron billets, and Co, Fe, Cu, and Si for the Starck billet. Examination of the Fe-Co phase diagram reveals no low-melting point phases. However, the contrary is true for the Co-Si and Fe-Si binaries. For Co-Si, liquid phases at temperatures ranging from 1195 to 1310°C extend across the diagram above 14 at.% Si. For Fe-Si above 32 at.% Si, liquid phases exist at 1200°C. Lower eutectic temperatures would be expected when Cu is also present with the above elements. The Co-Cu and Fe-Cu phase diagrams show broad solid solubility with the appearance of a liquid phase at ≃ 1100°C for most compositions. Furthermore, in the Cu-Si system, liquid phases exist at 800-850°C for most compositions above ≃ 12 at.% Si. Based upon this information, it is

very reasonable to assume that the Fe-Cu-Si and Co-Fe-Cu-Si chemistries present at the grain boundaries would indeed result in considerable softening of regions of the segregant above 600°C. The presence of carbon in the segregant, as will be discussed later, further supports this argument. It should be mentioned that chemical analyses of hot-pressed specimens showed Fe, Co, Cu, and Si levels which closely matched those in the starting powders. However, since the elemental distribution is non-homogeneous in the segregants, there is no single grain-boundary composition that can be identified. As a result, the volume fraction of the segregant that is soft or molten is very much dependent upon temperature. This accounts for the progressive decrease in bend strength and increase in intergranular fracture as the temperature is raised above 600°C.

The temperatures above which the strengths degraded for the unsieved-powder compacts were 800°C for the RMI and Ventron specimens and 1000°C for the Starck samples. It is clear that these temperatures are higher than those for the sieved materials because Cu is not present in the grain boundaries. However, the 200°C difference in degradation points must be explained. If only Co, Fe, and Si were present in the boundaries of the Starck TiC and only Fe and Si in the RMI and Ventron TiC, the Starck material would degrade at a lower temperature than the other two. However, the opposite occurs, and this can be explained by the presence of carbon in the grain-boundary segregants. The Co-C system shows a eutectic at 1309°C above 5 at.% C, but the Fe-C system exhibits a eutectic at 1147°C above ~ 8 at.% C. Thus, a Fe-C-Si system would be expected to show low-melting-point phases at lower temperatures than a Co-dominated Co-Fe-C-Si system. This would be especially true if there were insufficient carbon to reach the eutectic composition in the latter system. The most likely source of carbon would

be free carbon present in the starting powders. The as-received powders are believed to contain free carbon, but the Starck powder contains very much less free carbon than the RMI and Ventron powders. Hence, the likelihood that sufficient carbon is present to cause a significant drop in the temperature at which some softening begins is much greater for the RMI and Ventron materials. That circumstance and the low Fe content of the Starck TiC are the factors which account for the ≈ 200°C difference in degradation temperatures.

Recognizing the severity of the grain-boundary problem, experiments were undertaken for its alleviation. It was noted that for bend tests conducted at 1200°C and higher, a substantial fraction of the molten grain-boundary material exposed to vacuum upon fracture vaporized from the fracture surface. More of the segregant could be retained if the tests were conducted in argon. Figure 10 shows the segregant at the grain boundaries after testing of an STC-19 specimen at 1300°C in 1 atm argon.

These results raised the hope that the grain-boundary segregant could be removed from the as-hot-pressed TiC via grain-boundary diffusion to the surface and vaporization during a high-temperature vacuum heat treatment of the test bars. Only unsieved Starck powder compact specimens were so treated because of their better initial properties and their lower overall impurity content.

Table II shows the quantities of the major impurities present both before and after a vacuum (2×10^{-1} Torr) heat treatment of 10 hr at 2150°C. Significant reductions in the Co, Fe, Si, and O levels have been effected.

The W and Cr levels have not really changed, which is not surprising, since both form stable carbides. Discrete small (2-3 μm diam.) WC grains appear in the microstructure, and regions of segregated WC within the TiC grains and at triple points were detected in the STEM. The Cr was never microscopically located and was assumed to be more homogeneously dissolved in the TiC. Free carbon content could not be determined.

It is presumed that the Co, Fe, and Si levels were reduced during heat treatment by grain-boundary diffusion and vaporization. The change in oxygen content will be discussed later.

The microstructure and mechanical properties of the heat-treated TiC were consistent with the significant reductions in the grain-boundary constituents of the segregant. The grain-boundary films, so apparent before heat treatment, could not be observed in the SEM or TEM after heat treatment. Figure 11 shows the results of bend tests conducted on heat-treated specimens. Although low-temperature strength is degraded, mechanical integrity is maintained to temperatures much higher than those at which the as-hot-pressed material weakened. Further, the specimens exhibit plastic yielding above 1400°C. The yield-stress data of Fig. 12 represent the points at which the load-deflection curves deviated from linearity. Above 1400°C the yield stress is lower than the cleavage and/or grain boundary strength and, therefore, the specimens exhibit plastic deformation. Obviously, the near removal of the grain-boundary segregant significantly increased the high-temperature strength of the grain boundaries.

The bars which yielded were macroscopically bent, and TEM foils made from these specimens exhibited evidence of prior dislocation activity.

Figures 12 and 13 show the fracture surfaces of heat-treated specimens tested at room temperature and 1550°C, respectively. It is apparent that some grain growth has occurred during the heat treatment. The average grain size near the center of the specimens, where these photographs were taken, was ≃ 30 μm. However, the grain size decreases to ≃ 20 μm, moving from the mid-line of the bend bar to the surface. Apparently, the grain-boundary segregant, which is liquid during heat treatment, aids transport across the boundary and thus promotes grain growth. Since its concentration is highest along the mid-line of the bar during heat treatment, the final grain size is greatest there.

Two other salient features of Figs. 12 and 13 merit discussion. These are the extent of intergranular fracture and the appearance of significant grain-boundary porosity. Unlike the non-heat-treated material (see Fig. 3), the heat-treated specimens show about 50% intergranular fracture at room temperature. This indicates that although the high-temperature strength of the boundaries has been dramatically increased, the room-temperature strength has been somewhat reduced. From Fig. 13 it is apparent that the failure mode is almost totally intergranular. The heat treatment, therefore, raised the grain-boundary strength above the yield strength at 1500°C, but did not raise it above the cleavage strength.

The appearance of grain-boundary porosity in the heat-treated specimens is not fully understood. Quantitative metallography of as-hot-pressed and as-heat-treated specimens revealed that the heat-treated material contains an additional ≃ 1% total porosity. Concentration of large pores at the grain boundaries of the heat-treated samples was evident in the cross sections examined. Although sweeping of pre-existing pores

to the boundaries during heat treatment can contribute to enhanced boundary porosity, it cannot account for the additional total porosity. Two other possible phenomena would, however, increase the bulk porosity. First, the grain-boundary segregant which diffuses out of the material during heat treatment leaves behind the spaces it formerly occupied. These voids could spherodize to the pore geometries observed. However, the volume fraction of segregant present could account for only a small fraction of the additional ≃ 1% porosity. Given these circumstances, it is most reasonable to speculate that the grain-boundary porosity was caused by the evolution of a gas. The most likely candidate is $CO/C\theta_2$, formed by the reaction of dissolved oxygen with carbon in the grain boundary or the TiC itself. As indicated in Table II, oxygen content is significantly reduced during heat treatment. Hence, some of the gas evolved leaves the system via the grain boundaries. Gas which is entrapped causes the spherical grain-boundary voids. Should CO/CO_2 be the culprit, its evolution would reduce the carbon content of the segregant and thus facilitate the increase in high-temperature boundary strength as previously discussed.

Regardless of its cause, the grain-boundary porosity is real. Furthermore, there is evidence of pore coalescence along the boundaries (see Fig. 14). These larger pores and/or much larger grains probably act as strength-limiting flaws which account for the reduction in low-temperature strength of the heat-treated material.

The grain-boundary strength is not so critical when specimens are tested in compression. For this reason, a few compression tests were performed

on heat-treated material. The results agreed well with the data shown in Fig. 12. The yield strengths at 1200, 1400, and 1550°C were 370, 262, and 172 MPa (54, 38, and 25 ksi) respectively. These data are consistent with those obtained by Das, et al. [7], for TiC of this grain size. It is thus apparent that when the yield strength exceeds or equals the fracture strength in bending (1200 and 1400°C), no plastic deformation is observed in bending. However, when the bend strength exceeds the yield strength, plastic deformation is observed at about the same stress level in bending as in compression. Thus, the heat treatment to remove the grain-boundary segregant strengthened the boundaries of the high-temperature strength sufficiently that yielding was observed above 1400°C in four-point bending.

4. CONCLUSIONS.

1. Commercially available TiC powders contain impurities which segregate to the grain boundaries when the powders are hot pressed. These impurities which include Fe, Co, Si, and free carbon form low-melting-point phases which degrade the high-temperature strength.

2. Sieving the as-received powders in Cu sieves causes Cu transfer to the powder. This element also segregates to the grain boundaries and reduces the temperature at which strength degradation begins.

3. High-temperature vacuum heat treatment of as-hot-pressed material significantly reduces the levels of impurities at the grain boundaries. This, in turn, causes a dramatic improvement in high-temperature strength.

4. When the grain boundary and cleavage strengths exceed the yield strength, plastic deformation is observed at about the same stress level in bending as in compression.

5. Heat-treated polycrystalline Starck TiC of average grain size ≃ 25 μm possesses a D-B transition in bending at ≃ 1425°C.

REFERENCES

1. W. S. WILLIAMS and R. D. SCHAAL, J. Appl. Phys. 33, 955 (1962).
2. W. S. WILLIAMS, J. Appl. Phys. 35, 1329 (1964).
3. D. K. CHATTERJEE, M. G. MENDIRATTA, and H. A. LIPSITT, J. Mater. Sci. 14, 2151 (1979).
4. F. KEIHM AND R. KEBLER, J. Less Common Metals 6, 484 (1964).
5. A. KELLY and D. J. ROWCLIFFE, J. Am. Ceram. Soc. 50, 253 (1967).
6. K. HARA, H. YOSHIMAGA, and S. MOROZUMI, Japan Metals J. 42, 1039 (1978).
8. G. DAS, K. S. MAZDIYASNI, and H. A. LIPSITT, J. Am. Ceram. Soc. 65(2), 104 (1982).

LIST OF FIGURES

Figure

TABLE I

AS-RECEIVED POWDER-IMPURITY CHEMISTRY (wt ppm)

	STARCK	RMI	VENTRON
W	6500	1600	3600
Co	1200	15	10
Fe	545	3300	2550
Cr	425	470	430
Ni	40	10	10
Al	15	30	200
Cu	15	50	15
Si	45	95	80
Mo	75	20	100
Zr	10	35	50
Ca	30	20	30
O	2400	4300	4100
Free C	250	2150	4500

TABLE II

IMPURITY CHEMISTRY OF AS-HOT-PRESSED AND HEAT-TREATED

(2150°C, 10 HR, 2×10^{-1} TORR)

STARCK SPECIMENS (wt ppm)

	AS H.P.	AS H.P. & H.T.
W	6800	7100
Co	1300	200
Fe	505	280
Cr	450	420
Si	75	45
O	2800	1100

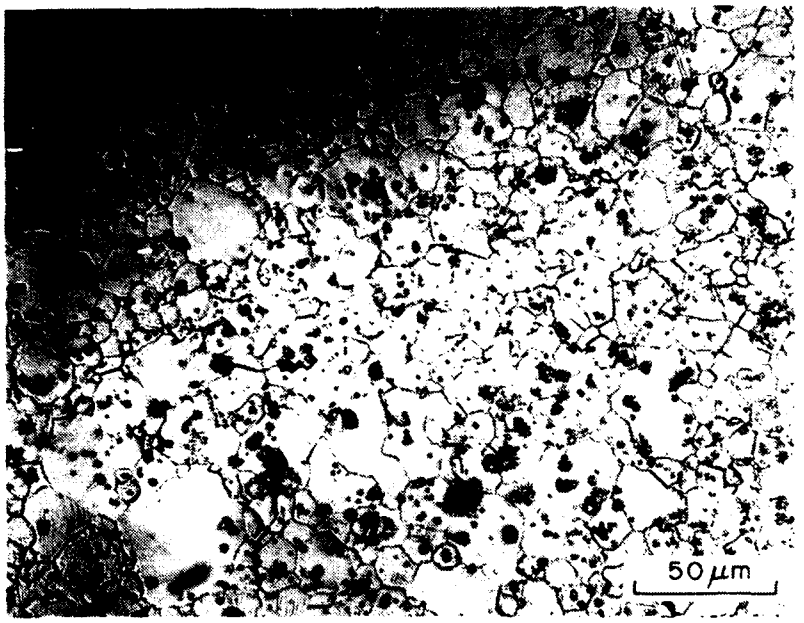

Figure 1

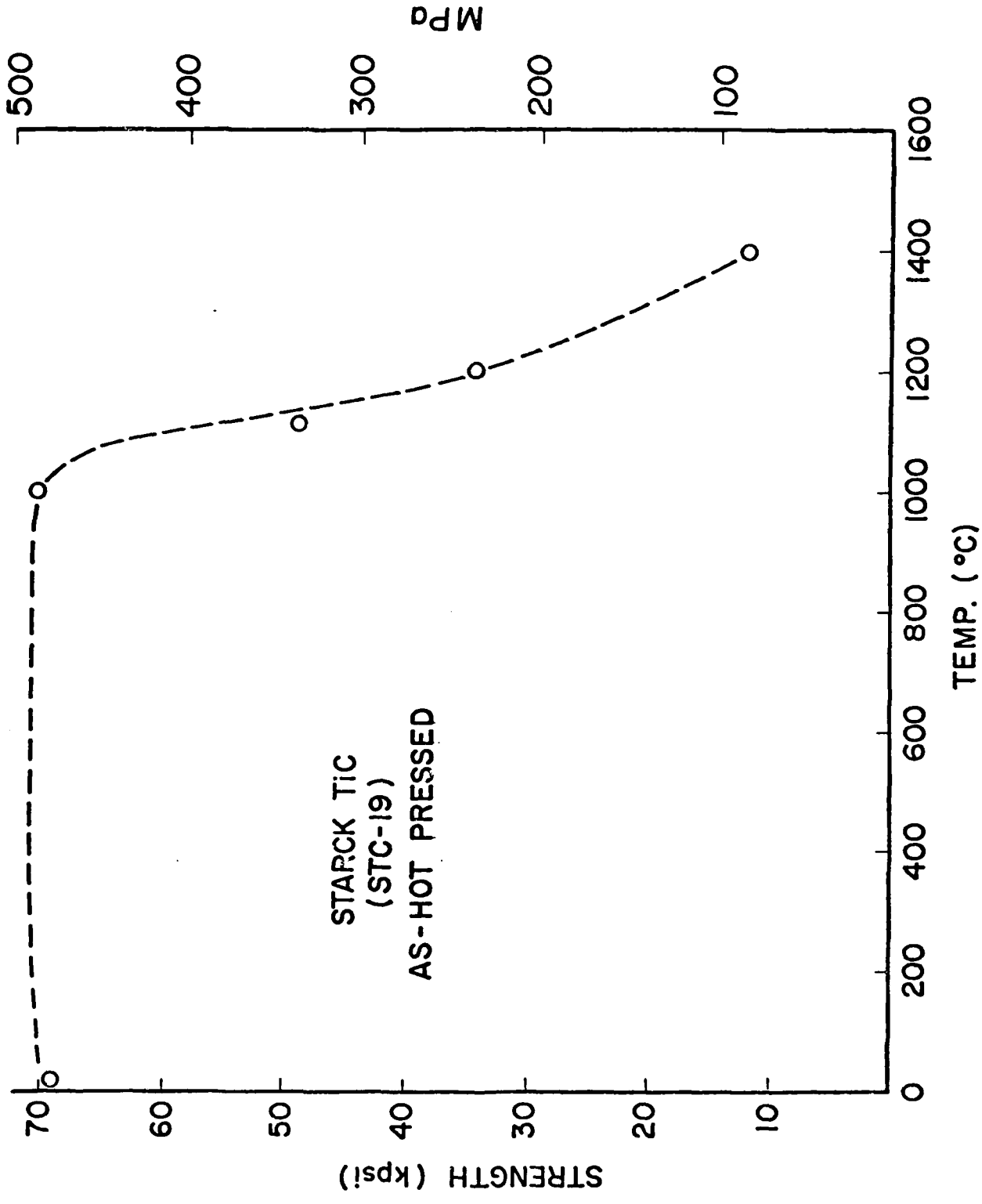
MPa
500
400
300
200
100
1600
1400
1200
1000
800
600
400
200
0
TEMP. (°C)
STARCK TiC
(STC-19)
AS-HOT PRESSED
70
60
50
40
30
20
10
STRENGTH (kpsi)

Figure 2

Figure [illegible]

Figure 5

Figure 6

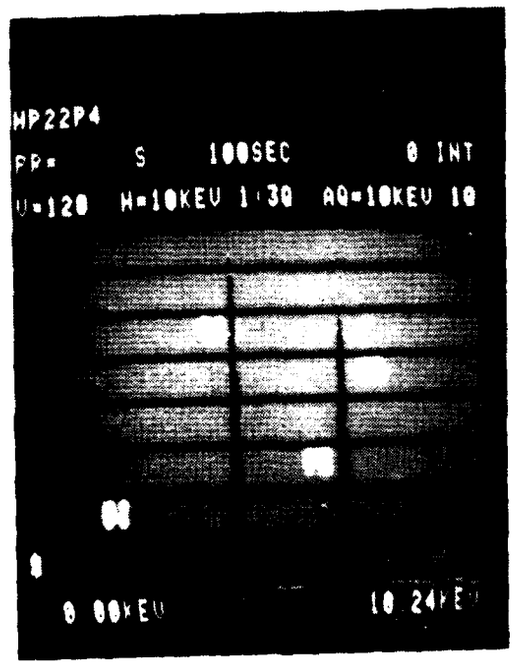
HP22P4
PP=
S
100SEC
0 INT
U=120
H=10KEU 1:30
AQ=10KEU 10
0.00KEU
10.24KEU

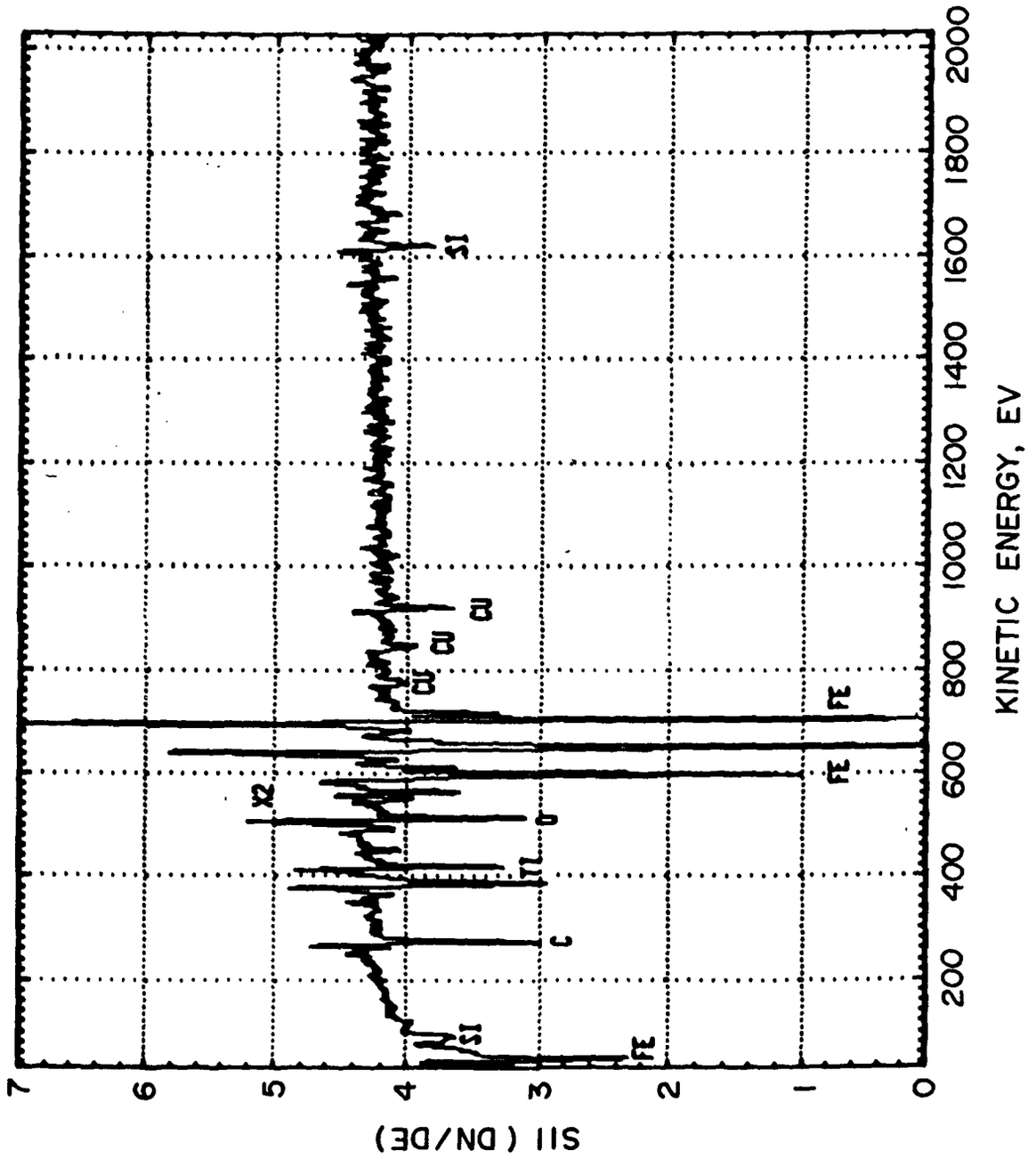
SII (DN/DE)
KINETIC ENERGY, EV
0
1
2
3
4
5
6
7
200
400
600
800
1000
1200
1400
1600
1800
2000
FE
FE
FE
FE
SI
SI
CU
CU
CU
O
C
N
X2

Figure 8

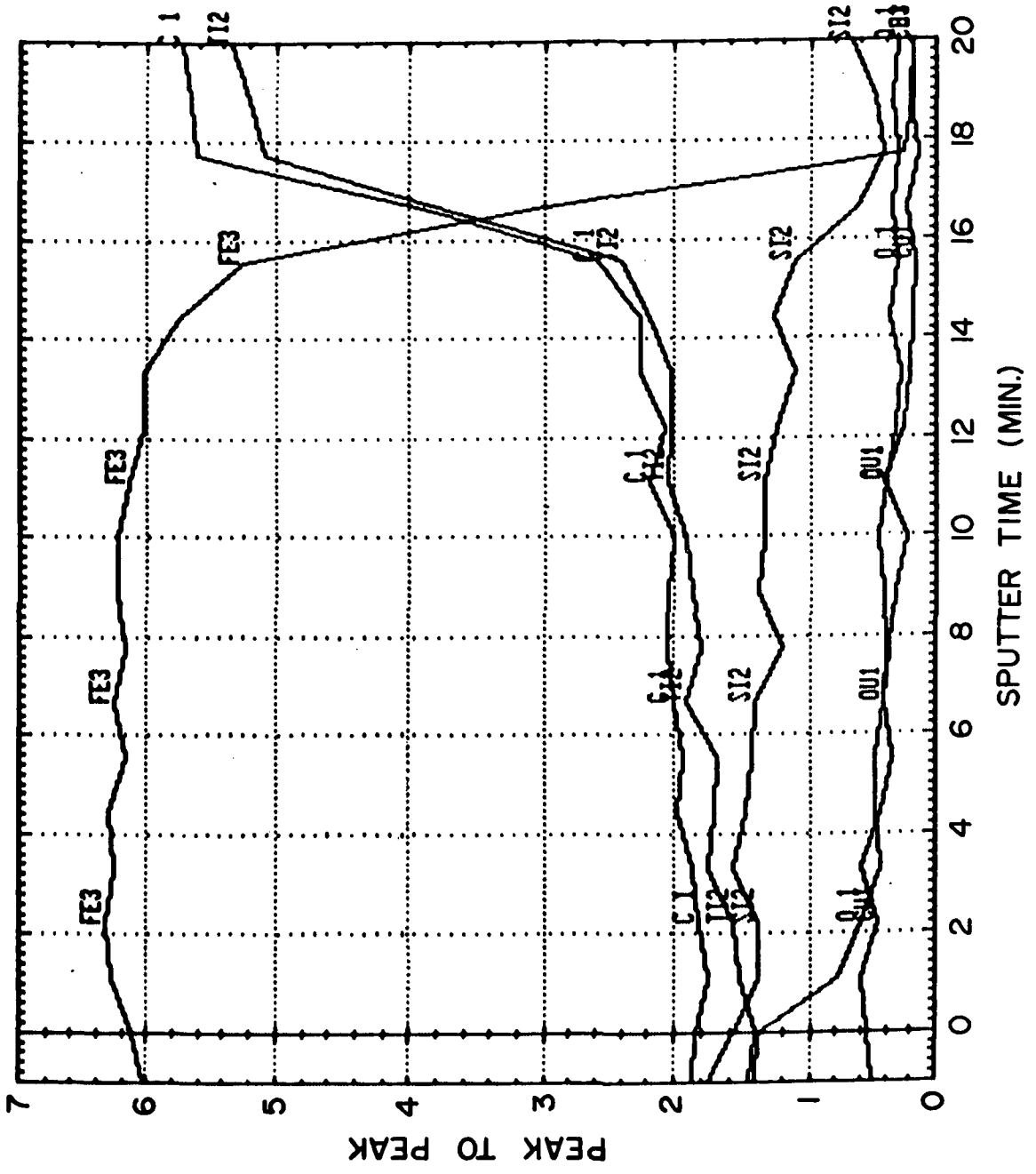

Figure 9

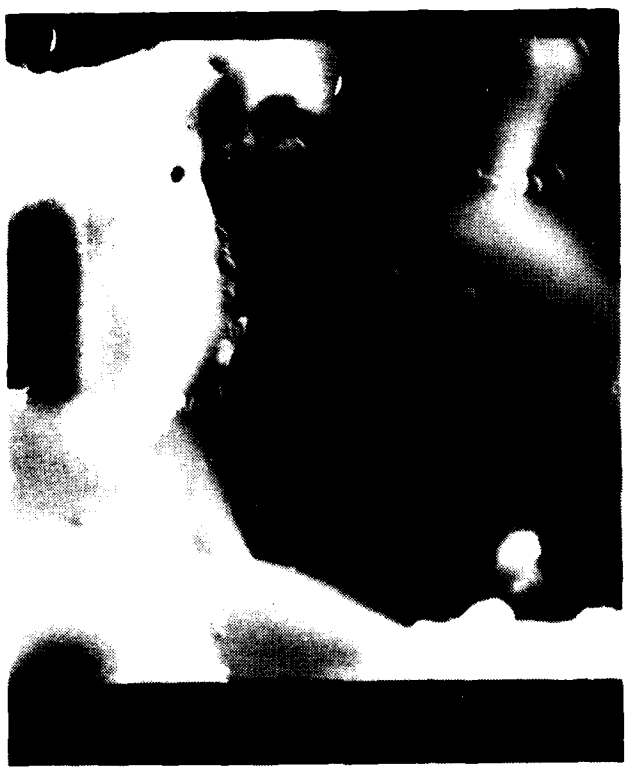

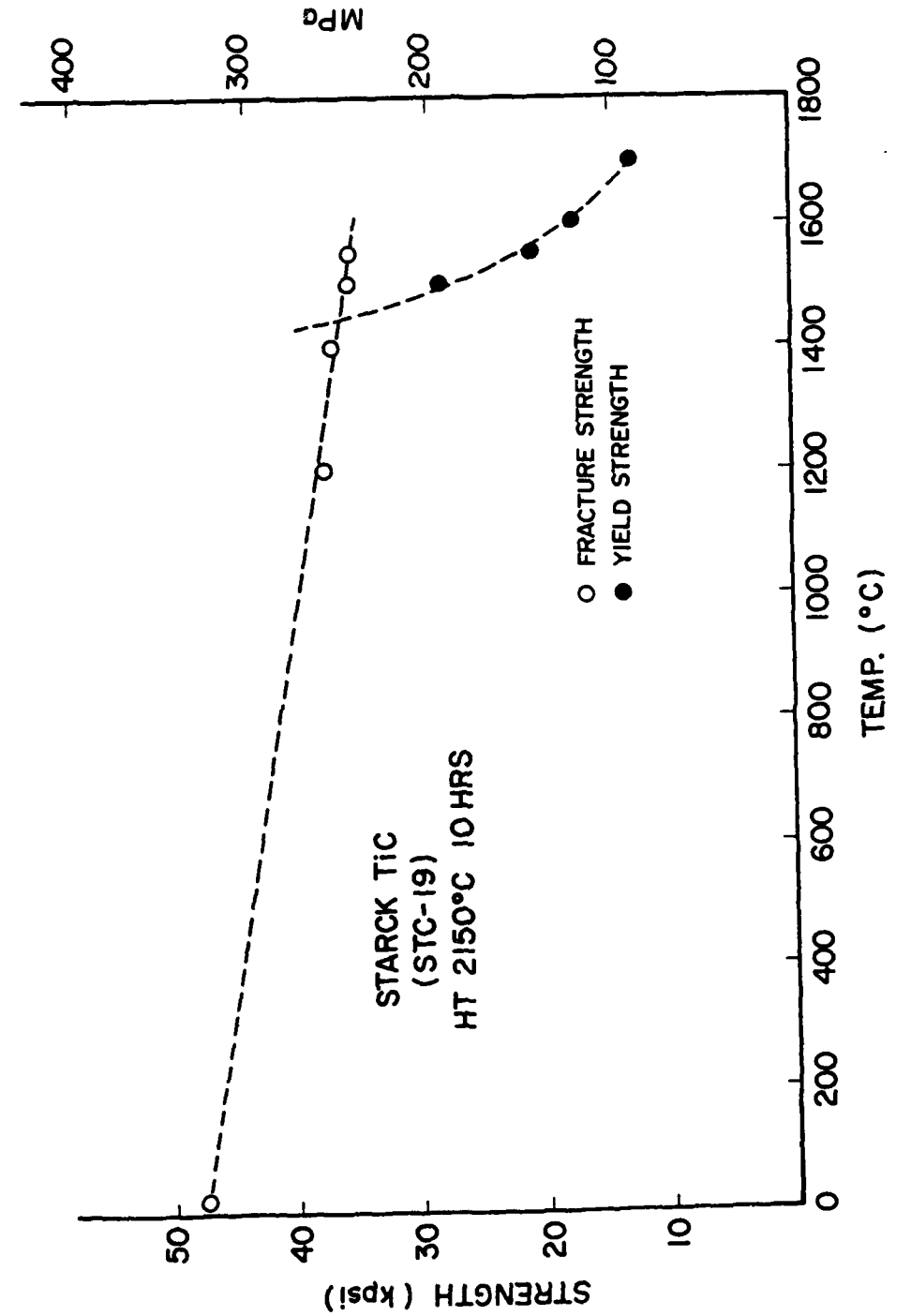
MPa
400
300
200
100
1800
1600
1400
1200
1000
800
600
400
200
0
TEMP. (°C)
O FRACTURE STRENGTH
● YIELD STRENGTH
STARCK TiC
(STC-19)
HT 2150°C 10 HRS
50
40
30
20
10
STRENGTH (kpsi)

Figure 11


DAT
FILM